2012-08-09

Development of a Method to Study Thromboembolism by Direct Observation in Blood-Contacting Microsystems Using High-Definition Video Microscopy

Yong Min Kim
Brigham Young University - Provo

Development of a Method to Study Thromboembolism by Direct Observation in Blood-Contacting Microsystems Using High-Definition Video Microscopy

Yong Min Kim

A thesis submitted to the faculty of
Brigham Young University
in partial fulfillment of the requirements for the degree of

Masters of Science

Kenneth A. Solen, Chair
William G. Pitt
Sivaprasad Sukavaneshvar

Department of Chemical Engineering

Brigham Young University

December 2012

ABSTRACT

Development of a Method to Study Thromboembolism by
Direct Observation in Blood-Contacting Microsystems
Using High-Definition Video Microscopy

Yong Min Kim
Department of Chemical Engineering
Masters of Science

A unique and novel method to study thromboembolism by direct observation was developed. High-definition videos of thrombus formation and embolization were successfully obtained in miniature flow cells using in-vitro, non-invasive, real-time techniques. Critical parameters of thromboembolism such as thrombus growth rate, thrombus growth direction, shear force on the thrombus at embolization, and adhesion strength of the thrombus to the foreign surface were determined.

Thrombus growth was found predominantly in two locations: 1) in the flow recirculation zone just after the trailing edge of the small tubes (53%) and 2) at the leading edge of the small tubes (47%). In the small tubes, thrombus volume and shear force acting on the thrombus increased in a power-law like function of time. In the large tubes, thrombus volume and shear force acting on the thrombus increased in a linear like function of time. The slope of thrombus growth rate in the small tubes was significantly greater than that in the large tubes. Thrombus growth direction was also estimated by tracking the thrombus center of mass with respect to time and typically ranged from 15 to 35 degrees from the direction of flow.

According to observations, embolization seems to occur via two possible mechanisms: 1) complete detachment of the thrombus by sliding off the foreign surface or 2) partial embolization of the thrombus by internal tearing. The estimated shear force on the thrombus at embolization was determined and was significantly greater in the small tubes than in the large tubes. The adhesion strengths of thrombi were calculated for the small tubes using the shear force at embolization and the estimated thrombus attachment area and ranged from 9.63 to 28.83 N/m^2 (mean = 16.24 ± 2.59 N/m^2 95% confidence), which was in good agreement with published results of platelet retention experiments.

An experimental series demonstrated that the developed method could be used to study the effects of controlled variables on thromboembolism parameters. In that series, heparin concentration in blood, blood flow rate, and device design were studied one variable at a time to test their effects on thrombus growth parameters and adhesion strength. Because of the small number of data, these preliminary results were statistically insignificant but pointed the way for future studies.

Keywords: Yong Min Kim, thrombosis, thromboembolism, blood-contacting devices

TABLE OF CONTENTS

LIST OF FIGURES

LIST OF TABLES

CHAPTER 1: INTRODUCTION

Blood-contacting devices are becoming increasingly more integral to the field of medicine. They are used in applications such as cardiopulmonary bypass surgeries, hemodialysis, vascular stents and shunts, and artificial hearts [1-3]. Even though significant progress has been made in developing blood-contacting devices over the past 50 years, such devices are limited in their effectiveness because of adverse blood-material interactions. The most common problem that occurs in these devices is thromboembolism, which results when blood contacts a foreign surface [4].

The phenomenon of thromboembolism can be divided into two parts: thrombosis (thrombus formation) and embolism (thrombus detachment). Thrombosis is the accumulation of blood platelets either within blood vessels or on the surfaces of biomaterials. Thrombus formation naturally occurs within the body when a blood vessel is injured and is beneficial because it creates a hemostatic plug and arrests bleeding. However, if thrombi are formed when a patient's blood comes into contact with a foreign surface in a blood-contacting device and subsequently embolize downstream, they can cause a blockage of blood circulation to vital organs, causing local ischemia, coronary occlusion, or stroke.

Thrombosis that occurs in blood-contacting devices begins with the adsorption and successive accumulation of plasma proteins along the foreign surface, followed by platelets adhering to the protein layer or existing thrombi [5]. As a thrombus grows, its adherence to the

foreign surface can be overcome by hemodynamic shear forces acting upon it. Detachment of the thrombus from the surface is known as embolism. Free-floating segments of thrombi are commonly referred to as thromboemboli, or simply emboli. The most common method of preventing thromboembolism within blood-contacting devices is to use anticoagulants such as heparin. Overuse of these blood additives, however, can cause hemorrhagic and/or other drug-related disorders [6]. Additionally, they don't completely inhibit platelets or eliminate thromboembolism.

Thromboembolism is difficult to understand due to the many variables that add to the complexity of the phenomena. Patient-specific factors such as blood composition, diet, and medication can have a major impact on thromboembolism. Other factors such as surface chemistry between the blood and various biomaterials, changes in hemodynamic conditions, and complexity of device design increase the difficulty of studying thromboembolism. Many contributing factors of thromboembolism have been investigated in previous decades; however, the overall understanding of thromboembolism in blood-contacting devices is still very limited.

The research presented in this thesis is a continuation of previous research conducted by Goodman, *et al*. [7]. Their study used video microscopy to observe thromboembolism in an in-vitro model that mimicked a blood-contacting device. They also developed a system to detect and analyze emboli in real time using a light-scattering microemboli detector (LSMD) and constant pressure filtration (CPF).

The overall goal of this research was to develop a method to study thromboembolism in blood-contacting devices by direct observation, and then use the developed method to gain a better understanding of the characteristics of thromboembolism by estimating critical parameters such as growth rate, growth direction, shear force on the thrombus, and adhesion strength. An

additional goal was to demonstrate that the developed method could be used to study the effects of controlled variables such as heparin concentration, flow rate, and device design on these critical parameters of thromboembolism.

CHAPTER 2: BACKGROUND

2.1 Thrombus Formation

Within the human body, the formation of a thrombus most commonly results from one of two situations. First, a disruption in the normal state of homeostasis results in the activation and collection of platelets within a blood vessel. This is usually the result of a disease that causes the improper activation of platelets and coagulation pathways. Second, an injury can cause the activation of clotting factors, which leads to thrombus formation. External to the human body, when blood interacts with foreign surfaces in blood-contacting devices during medical procedures, thrombus formation occurs frequently and is a leading cause of complications when these devices are used.

2.1.1 Normal Physiological Conditions

Under normal physiological conditions, thrombus formation does not occur due to the thrombosis-resistant characteristics of the endothelial inner-lining of blood vessels [8]. The non-thrombogenic characteristics of the endothelium are caused by several factors. First, both endothelial cells and platelets are highly negatively charged, and they repel each other [9]. Second, endothelial cells synthesize prostacyclin I_2 (PGI_2), which inhibits platelet aggregation [10]. Endothelial cells also release thrombomodulin and heparin sulfate which are cofactors that inhibit thrombin activity [11-12]. Thrombomodulin increases the ability of thrombin to activate protein C, which in turn inactivates factor Va and factor VIIIa and causes a decrease in thrombin

concentration [13]. Endothelial cells can also release tissue plasminogen activators, which in the presence of fibrin, initiates fibrinolysis and inhibits thrombus formation [9]. A summary of the thromboresistant properties of the endothelium is shown in Figure 1.

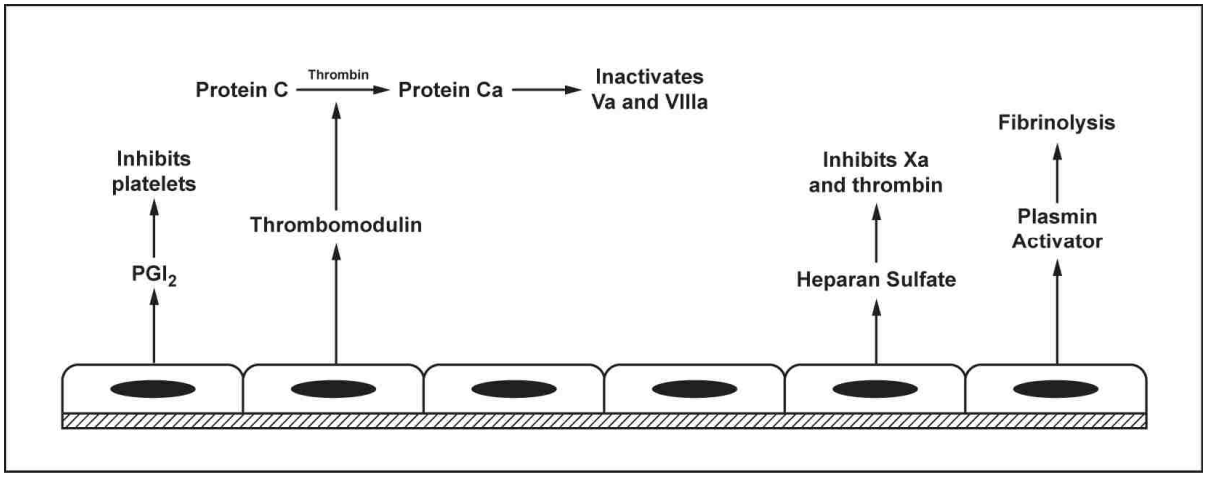

Figure 1: Thromboresistant properties of the endothelium.

2.1.2 Blood Flow Response to Injury

When an injury, inflammation, or endothelial dysfunction occurs in a blood vessel, a three-step mechanism ensues in order to arrest bleeding. First is the vasoconstriction of a damaged blood vessel in order to slow blood loss [14]. Second is the formation of a platelet plug. This occurs when the endothelial wall is damaged and the blood is exposed to subendothelial collagen at the damaged location. The collagen promotes platelet adhesion at the damaged site, and the combination of this contact and other rheological factors causes platelets to become activated [15]. Activated platelets release chemicals such as adenosine diphosphate (ADP) and thromboxane A_2, which then activate other platelets and lead to the aggregation of more platelets to the damaged site [16-17]. This process is illustrated in Figure 2.

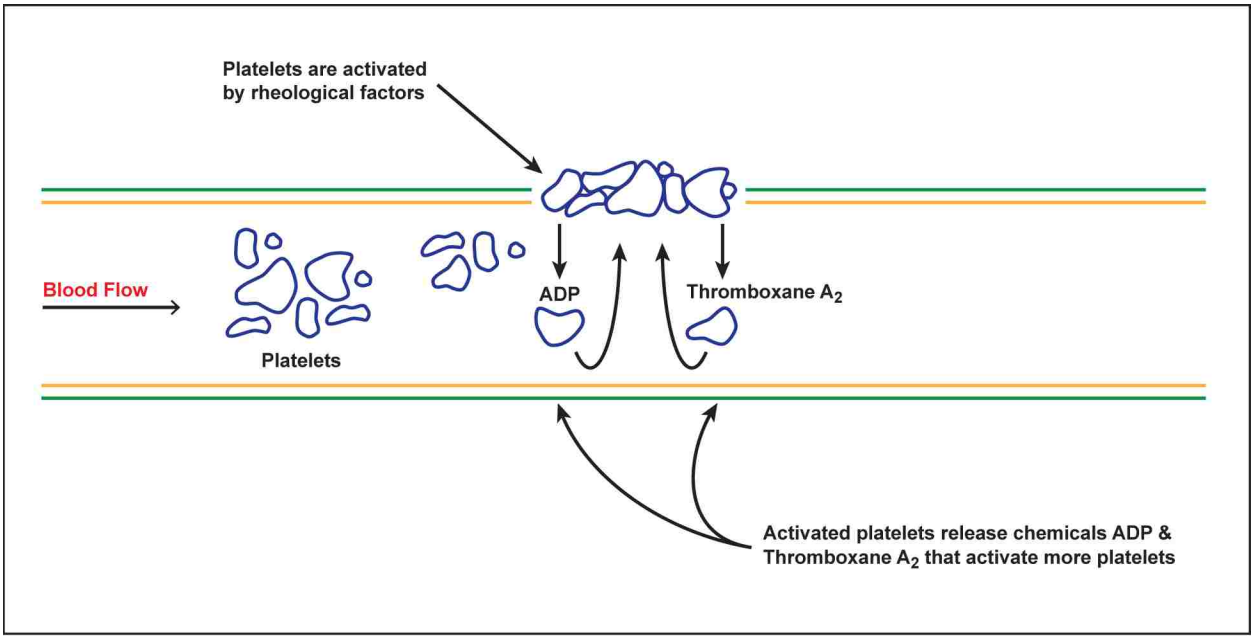

Figure 2: Formation of a platelet plug after an injury to the blood vessel.

The final step in the three-step mechanism is coagulation. There are over dozen clotting factors that exist in the blood. These clotting factors are proteins that, under normal conditions, are inactive. When an injury occurs to a blood vessel, these clotting factors are activated in a cascading sequence, with one clotting factor activating a second, which then activates a third and so on [14]. The clotting cascade is shown in Figure 3.

As illustrated in Figure 3, both intrinsic and extrinsic pathways can result in the activation of factor X. Factor X activates the prothrombin activator which converts prothrombin to thrombin. Thrombin then acts as an enzyme to turn fibrinogen to fibrin. Fibrin fibers form a loose mesh network. Factor XIII stabilizes the fibrin to form dense fibrin polymers, and by trapping erythrocytes and platelets a blood clot is formed [14]. This natural process of thrombus formation in the body is very similar to the interactions of blood with foreign surfaces outside of the human body. This phenomenon will be discussed in the next section.

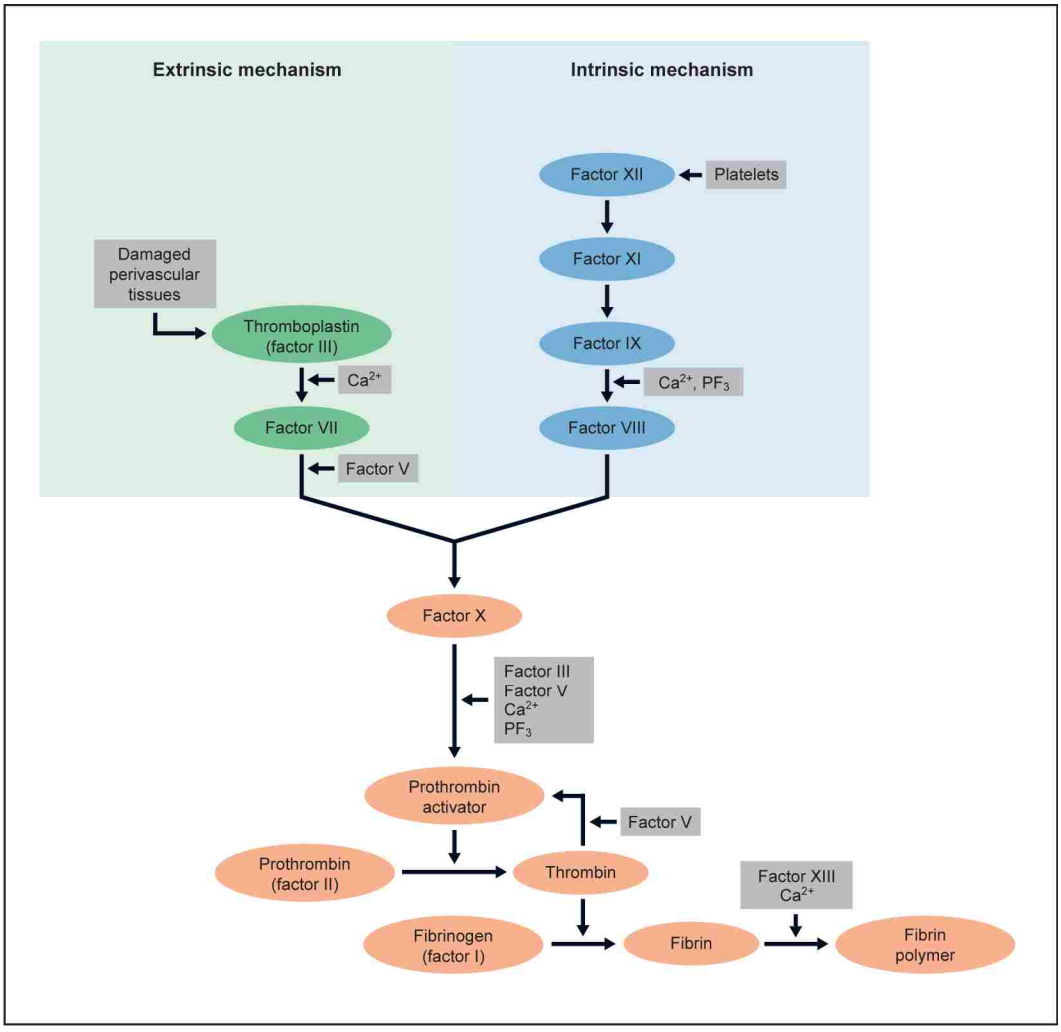

Figure 3: Simplified illustration of coagulation cascade [4].

2.1.3 Blood Flow Response to Foreign Surfaces

When blood comes into contact with a foreign surface that is non-endothelial in nature, the proteins in the blood first adsorb onto the artificial surface [18-20]. At the same time, blood platelets are activated by coming into contact with the foreign surface and other rheological factors. Activated platelets begin to adhere to the protein layer created by protein deposition. Activated platelets also promote further platelet adhesion by releasing agents such as ADP, thromboxane A_2, and thrombin, which activate and attract more platelets to the site of the

thrombus formation and stimulate the coagulation cascade [21]. This process is illustrated in Figure 4.

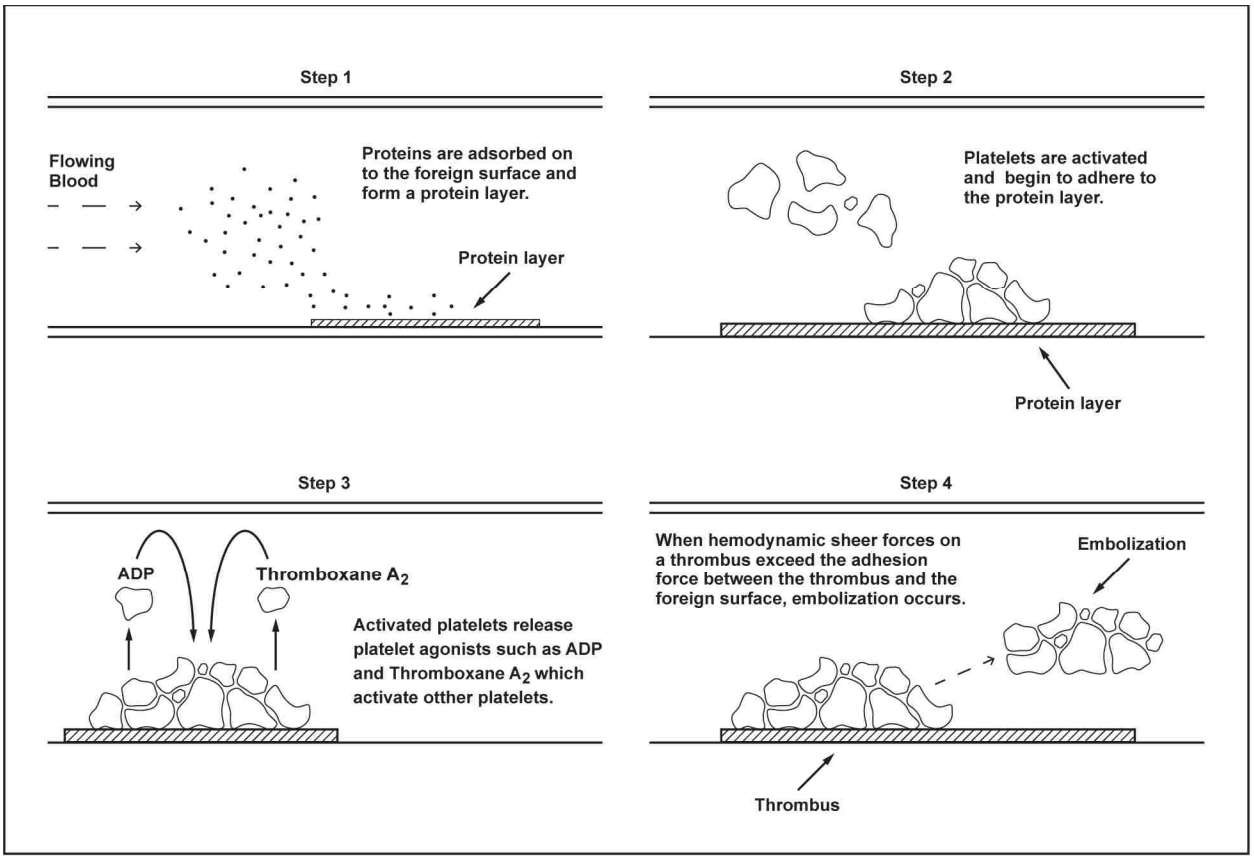

Figure 4: Mechanism of thromboembolism in blood-contacting devices.

2.2 Embolization

As the thrombus grows, the shear force on the thrombus increases due to the reduction of the cross-sectional flow area. When these hemodynamic shear forces become greater than the adhesion strength of the thrombus to the foreign surface, the thrombus detaches from the surface. This process creates a free-floating particle in the blood, often referred to as an embolus or thromboembolus. Depending on the size and cohesive strength of the embolus, it may become

broken up into harmless smaller parts, reattach to another surface or thrombus, or lodge in smaller vessels downstream, which can result in serious complications due to vessel blockages.

2.3 Fluid Dynamics of Thromboembolism

While there are many factors that contribute to thromboembolism, the dynamics of blood flow within a blood-contacting device is believed to be one of the most important factors. Fluid dynamics of blood flow facilitate the transport of platelets and other reacting agents to the surface of biomaterials and existing thrombi by mass-transfer methods of diffusion and convection. In addition, platelets and other reacting agents are known to be activated by shear stresses within the blood flow [22]. Last, the most important factor of embolization of thrombi is considered to be the shear force on the thrombus.

2.3.1 Diffusion

Diffusion is one of the primary methods of transfer for platelets and other blood components to a foreign surface and to an existing thrombus. Diffusion of platelets and other blood components may be increased by the presence and rotation of erythrocytes (red blood cells) caused by shearing blood flow [23-24]. An increase in apparent platelet diffusivity enhances the rate of platelet adhesion to foreign surfaces and to existing thrombi, thus increasing the rate of thrombus growth.

2.3.2 Convection

Under normal conditions in the body, the convection of blood components toward a surface is minimal as most blood flow in the body is laminar. The exception is at locations where vessels branch or constrict. Similarly, in blood-contacting devices, the convective

transport of platelets and other blood components toward the surface of a biomaterial is induced by curvature and/or abrupt changes in the cross-section of a flow [25].

At these locations, convective forces within the blood flow introduce secondary flow effects that transport platelets and other reacting agents closer to the foreign surface and existing thrombi. In cases where there is a dramatic disruption of the flow stream, flow separation occurs and causes the momentum of the main stream to rotate, creating flow recirculation zones. An illustration of this phenomenon is shown in Figure 5. Blood in the recirculation zones experiences increased residence time, which allows longer exposure of thrombogenic agents to foreign surfaces and existing thrombi [26].

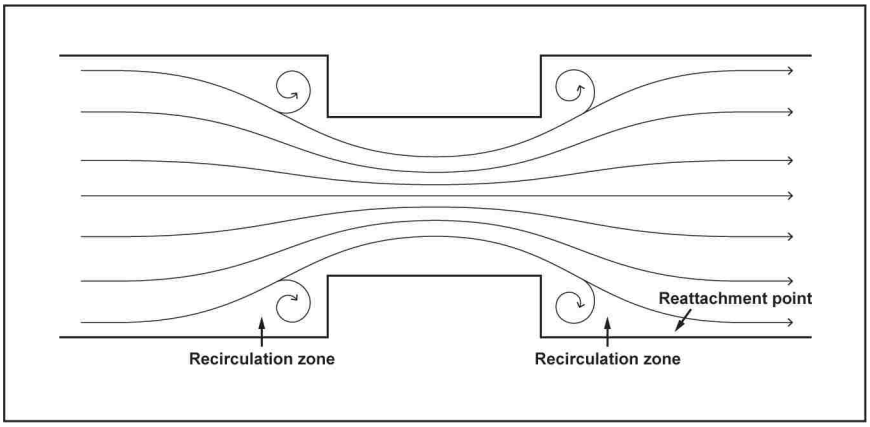

Figure 5: Recirculation zones created due to flow separation.

As a thrombus develops, it may cause local flow disturbances that further increase the convective transport of platelets and other blood components to the existing thrombi or to the foreign surface, leading to an increase in thrombus growth. Also, an existing thrombus may create a recirculation zone on the back side of the thrombus, leading to an increase in thrombus growth [27]. This is illustrated in Figure 6.

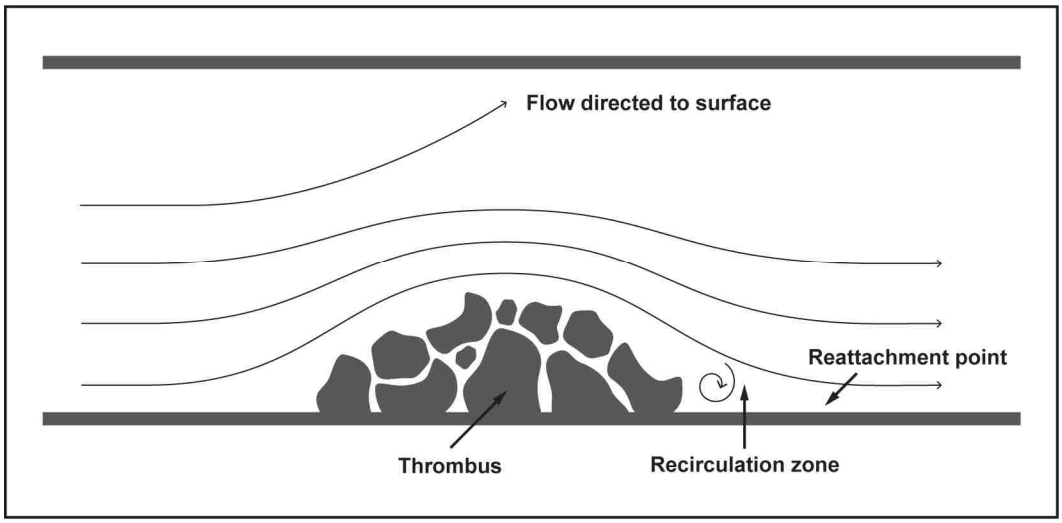

Figure 6: Flow disturbances caused by an existing thrombus.

2.3.3 Shear Stress

Shear stress within blood flow is often considered to be one of the most important fluid dynamic factors that affect thromboembolism. Shear stress causes red blood cells to rotate, which increases the apparent diffusivity of platelets and other blood components to the surface of the biomaterials or the existing thrombi [28]. Shear stress is also considered as one of the main causes that activates platelets through deformation [29-30]. Even at shear stress less than 10 Pa, platelets release components such as ADP, thromboxane A_2, and thrombin, which leads to increased platelet surface adhesion and aggregation [31-32].

Shear stress is also a major factor for embolization. As the thrombus grows, it experiences an increase in shear force due to the increased surface area that is exposed to the blood flow. If the shear force on the thrombus exceeds the adhesion force between the thrombus and the biomaterial surface, embolization will occur.

The shear force on the thrombus can be quantified using the following equation:

$$F = \tau \cdot A \tag{1}$$

where *F* represents the shear force on the thrombus, A is the surface area of the thrombus adjacent to the flow, and τ is the shear stress acting on the thrombus. The shear force can be estimated by applying Eq. 1 to differential slices of the thrombus and summing the resulting pieces, as expressed in Eq. 2.

$$F = \sum (\tau \cdot A_s) \tag{2}$$

where A_s represents the surface area of a slice of the thrombus.

For Newtonian fluids, shear stress, τ, can be described by the following equation:

$$\tau = \mu \underline{\dot{\gamma}} \tag{3}$$

Assuming a one-dimensional flow of Newtonian fluid, shear stress can be described by the linear relationship:

$$\tau = -\mu \cdot \frac{dv}{dl} \tag{4}$$

where μ represents the viscosity of the blood and $\frac{dv}{dl}$ represents the rate of change of fluid velocity with respect to the perpendicular distance from the thrombus surface.

2.4 Pharmacological Agents

Due to the damaging consequences of an embolus lodging in a blood vessel and blocking blood flow, the use of pharmacological agents to minimize thrombus formation is often used in clinical environments. These pharmacological agents are either anticoagulants or antiplatelet agents (i.e. platelet inhibitors).

Heparin has become the most commonly used anticoagulant in both clinical and research settings [33]. Heparin works by binding and activating antithrombin III. Active antithrombin III then inactivates thrombin and other factors that contribute to coagulation, including factors Xa, XIa, and IXa. Antithrombin III then forms a 1:1 irreversible complex with the coagulation

enzymes, and the heparin dissociates from the complex. Dissociated heparin can be reused to bind and activate antithrombin III. The anticoagulant activity of heparin is useful in situations where clot formation must be prevented; however, it will not actively break up already existing thrombus clots [33-34].

Warfarin is also a common anticoagulant used following the implantation of cardiovascular devices, such as vascular grafts and artificial valves. Warfarin works by interfering with the blood's vitamin K cycle by reducing the production of vitamin K-dependent coagulation proteins such as prothrombin, Factor VII, Factor IX, and Factor X [35].

Another commonly used pharmacological agent is aspirin, which is a platelet inhibitor. Aspirin is used for therapeutic purposes after various cardiovascular surgeries in order to prevent potential thromboembolism-related issues such as heart attack and stroke. Clopidogrel (better known as Plavix) is also used for a similar purpose. This agent works by blocking ADP aggregation, whereas aspirin inhibits platelet activation by irreversibly inactivating platelet cyclooxygenase [36].

Due to undesirable complications such as hemorrhaging, the use of anticoagulants and/or antiplatelet agents in clinical situations must be well-controlled. Optimal levels of these agents are unique for each individual in each situation, and understanding their effects on thrombus growth and embolization requires further research.

2.5 Previous Research on In Vitro Model Microsystems

As part of an ongoing research at Brigham Young University, a low-volume *in vitro* model that observes thrombus growth and embolization has been developed and improved over the past 15 years [7]. In this model, fresh human blood is passed through a miniature flow cell

that mimics a blood-contacting device, and thromboembolism is visualized and detected continuously through non-invasive techniques.

The flow cell was originally built by inserting four 1 mm segments of Teflon tubing into 1/32 inch I.D. PVC tubing with 1 mm of space between each segment. The flow rate of the blood through the flow cell was set at 3 mL/min using a syringe pump, while the temperature of the blood was held constant at 37°C. This model was designed to produce repeatable flow disturbances that caused a high level of rotational flow, thus increasing the transport of platelets and other blood components to the wall and the shear stress within the flow.

Thromboembolism was then observed and recorded in real-time using video microscopy, as shown in Figure 7. Emboli were continuously detected using a light-scattering microemboli detector (LSMD) [37]. The LSMD monitors embolization by differentiating the light-scattering patterns created by emboli within the flow. As thrombi embolize and travel downstream through the transparent tube, laser light is directed into the tube, and the light scatters from the emboli. The change in magnitude of the light-scattering intensity is dependent on the size of the emboli. The LSMD captures the thromboembolism activity level by gathering the number and the size of the emboli.

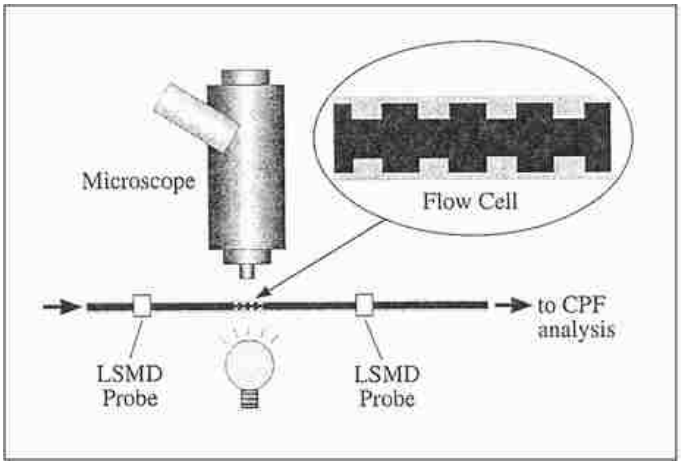

Figure 7: Goodman experimental model [7].

The relative strength of the emboli was determined by using a method of constant pressure filtration (CPF) [7]. About 1 mL of blood was collected from the end of the flow cell. This blood sample was then passed through a filter with 20 μm pores at a pressure 50 mm Hg. The relative strength of the emboli was determined by the amount of blood passed through the filter. If the emboli were large (larger than 20 μm) and/or strong, the blood did not pass through the filter due to clogging; however, if the emboli were weak and/or small (less than 20 μm), they passed through the filter or broke apart due to the applied pressure gradient.

The study results showed that thrombus growth was observed in areas with high rotational flow, such as at sharp corners and/or reattachment and separation zones [7]. This study demonstrated the potential of using a low volume *in-vitro* model to investigate the relationship between the nature of blood flow and the progression of thromboembolism in blood-contacting devices. It did not show, however, how certain change in flow properties or device design affected the thromboembolism characteristics.

CHAPTER 3: OBJECTIVES

The overall goal of this research was to develop a method to study thromboembolism in blood-contacting devices by direct observation using in-vitro, non-invasive, real-time techniques. The second goal was to use this method to gain a better understanding of the characteristics of thrombus formation, growth and embolization by estimating critical parameters such as growth rate, growth direction, shear force on the thrombus, and adhesion strength. The last goal of this research was to demonstrate that the developed method can be used to study the effects of controlled variables such as heparin concentration in blood, blood flow rate, and device design on these critical parameters. To accomplish these goals, the specific objectives of this study were set as follows:

1) Acquire high-definition video recordings of blood thrombus formation and embolization in miniature flow cells under various conditions from which characteristics of thromboembolism can be quantified.
2) Use image analysis software and the acquired videos to quantify critical parameters of thromboembolism: the thrombus growth rate, the thrombus growth direction (angle of growth vector at center of mass of thrombus relative to flow channel lumen), the shear force on the thrombus, and the adhesion strength of thrombus to the foreign surface.
3) Correlate these critical parameters of thromboembolism with changes in controlled variables: blood flow rate, heparin concentration level in blood, and device design.

CHAPTER 4: DEVELOPMENT OF EXPERIMENTAL MODEL

As noted in Section 2.5, the experimental set-up in this research was an extension of a previously developed model presented by Goodman *et al.* [7]. An overview of the experimental set-up can be seen in Figure 8. The experimental set-up was comprised of the following components: flow cell, syringe pump, high-definition video microscope, and light-scattering microemboli detector LSMD. These components are each described in detail in the following sections.

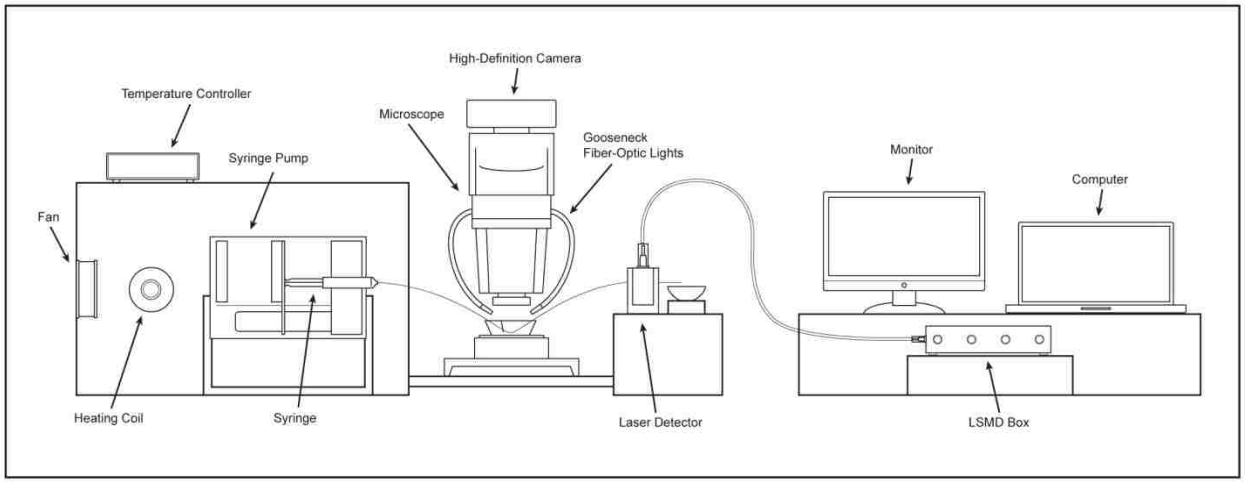

Figure 8: Illustration of experimental set-up.

4.1 Development of Flow Cell

Many flow cells that mimic blood-contacting devices have been developed in the past to study thromboembolism [38]. However, most flow cells developed previously did not create significant disturbances within the flow, which are necessary to increase the transport of platelets

and other blood components to the wall of the foreign surface. Therefore, an important aspect of this research was developing a flow cell that caused enough flow disturbances to help mimic the thromboembolism observed in real blood-contacting devices.

In this study, a cylindrical, translucent micro flow cell that mimics a blood-contacting device was prepared using a Miro-Renathane polyurethane tube from *Braintree Scientific*® (Braintree, MA). A 21-inch section of tubing (0.04" O.D. and 0.025" I.D.) was cut using a razor blade. Segments of tubing (0.025" O.D. and 0.012" I.D.) that were 1-mm in length were inserted into the larger-diameter tube, 8 inches from one end using a metal wire and warm water. The two small tubes were separated from each other by either 1 mm or 0.5 mm depending on the desired experimental condition. The small tube inserts created repeatable flow disturbances and thus increased the transport of platelets and other blood components to the surface of the biomaterial.

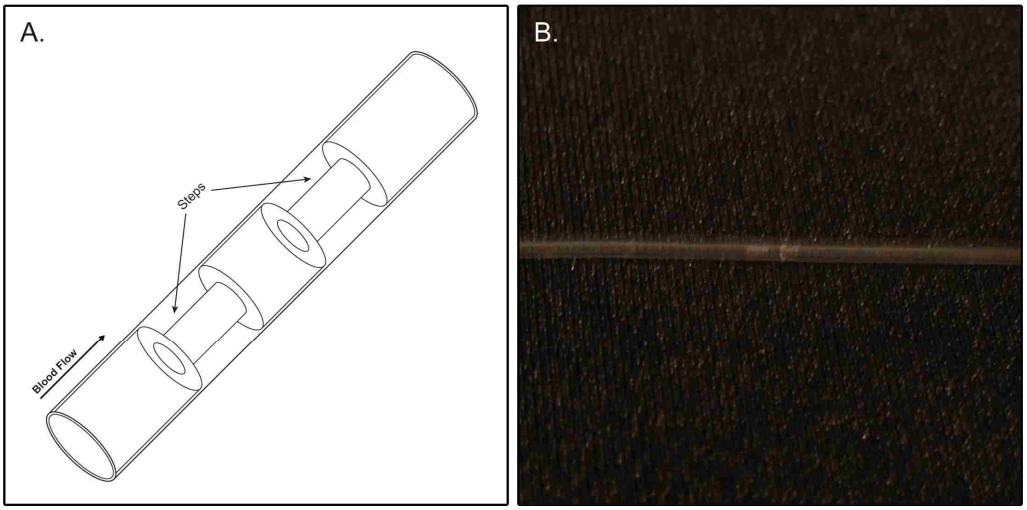

Figure 9: Small tube inserts in the flow cell A) illustration B) actual.

After insertion of the two small tubes, one end of the flow cell (not the end through which the steps were inserted) was threaded through a Luer connector and out the other side. In this way, the tubing actually protruded into the syringe, thus the blood contacted only the tubing

during the experiment. The Luer fitting was anchored and sealed with Parafilm® as shown in Figure 10.

Figure 10: Luer fitting attachment of the flow cell.

Before use, each flow cell was rinsed with a 5% ethanol-water solution, then rinsed with distilled water and allowed to dry to ensure no bacteria or other particles remained on the inside of the flow cell. After the flow cells were dry, the tips of tubing protruding from the Luer connectors were coated with a 100 unit/mL heparin/benzalkonium chloride solution and dried for a minimum of 24 hours. This preparation method of the flow cell helped to prevent any clotting from occurring at the connection between the syringe and the flow cell entrance region.

4.2 Syringe Pump Set-up

During the experiment, it was necessary to keep the blood at a constant temperature of 37^{o} C to avoid hypothermia. Therefore, the syringe pump was placed in a clear Plexiglas box with a heating coil and a fan to keep the blood in the syringe at 37^{o} C. It was also important to keep the blood well-mixed throughout the experiment to prevent the separation of plasma and red blood cells in the blood sample. To accomplish this goal, the syringe pump was attached to an apparatus which allowed the pump to be flipped 180^{o} every three minutes during the

experiment. If a certain donor's blood was known to separate more quickly than normal, the syringe pump was flipped every two minutes to minimize the settling or separation of the blood components.

The flow rate of the blood in the flow cell was controlled by the syringe pump with settings that could be changed to desired specifications. The desired settings allowed the syringe pump to push the blood sample into the flow cell at a constant flow rate. A detailed set-up of the syringe pump system used for the experiment is shown in Figure 11.

Figure 11: A) Syringe pump set-up B) Syringe pump rotation.

4.3 High-Definition Video Microscopy

A high-definition camera (*Cannon EOS Rebel T1i*) and microscope (*Bausch & Lomb, Stereozoom 7*) were used to make high-definition videos of thromboembolism occurring within the flow cell. First, the area of the flow cell containing the two small steps was secured under the microscope by placing the flow cell into a metal ring with a slit on each side. The metal ring was placed in a translucent plastic dish that was held above the base of the microscope by metal wires configured in the shape of the dish. This allowed the light to penetrate through the blood at all angles as it passed through the flow cell.

Two gooseneck fiber optic lights *(AO Scientific Instruments)* were used to illuminate the steps in the flow cell under the microscope. The optimum brightness was used to allow maximum transparency of the blood while minimizing any glare from the tubing. It is important to note that the flow cell was submerged in mineral oil, which has a refractive index (1.476-1.483) similar to that of polyurethane tubing (approximately 1.5) and enhanced the transparency of the blood flow.

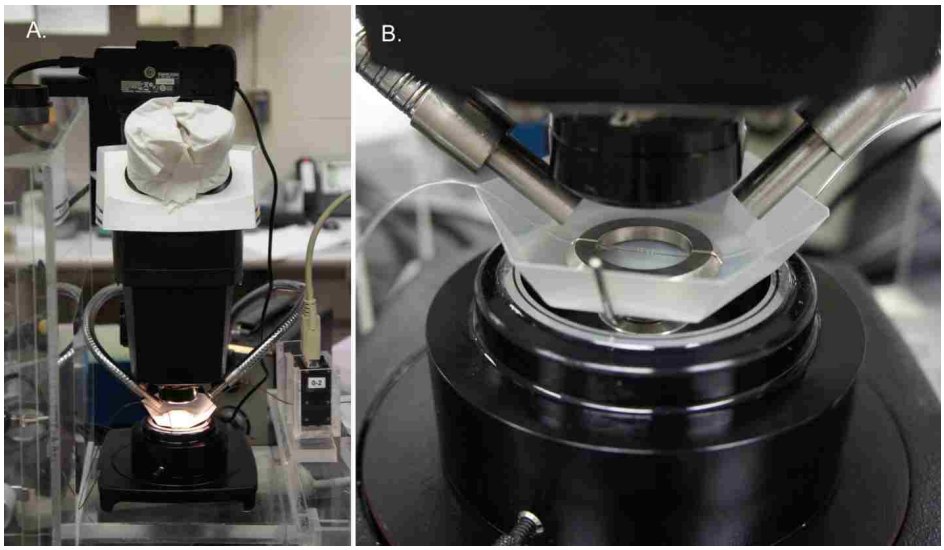

Figure 12: A) Set up of high-definition video microscopy B) Secured flow cell under the microscope.

The submerged flow cell was positioned under the viewing field of the microscope to capture the growth of a thrombus in the projected area with a high-definition camera. The recordings of the thrombus growth were viewed during the experiment on an HDMI Screen that was connected to the high-definition camera.

4.4 Light Scattering Microemboli Detector (LSMD)

As shown in Figure 8, the outlet section of the flow cell was placed into a laser cuvette. About one inch of tubing extended past this cuvette to allow the blood to drip from the end of the

tube into a plastic dish, which allowed for easy disposal of the blood at the end of the experiment. The laser cuvette contained one laser diode that shined straight down onto the flow cell and two detectors that determined the scattering of the laser light. Prior to all experimental runs, a base level of light scattering for unaltered blood was determined.

The light-scattering microemboli detector (LSMD) monitors embolization by differentiating the light-scattering patterns created by flowing emboli from red blood cells and other blood components within the flow cell [37]. As thrombi embolize and travel downstream through the flow cell, they pass through the laser light illuminating the tube. A detected change in magnitude of the scattered light intensity is dependent on the size of the emboli. Accumulation of size and number of the emboli in the flowing tube determines the thromboembolic activity level.

After the base level was determined, a *LabView®(National Instruments)* program was used to measure the amount of scatter relative to this level, giving an effective emboli count. When the syringe pump was flipped (as discussed in Section 4.2) the counting was turned off momentarily due to the fact that the action of flipping may cause some settled particles within the syringe to be released into the flow cell.

4.5 Blood Sample Preparation

Before blood was drawn from a donor, a syringe was prepared with the correct amount of heparin drawn from a stock 100 units/mL solution. The fluid concentration was usually specified to be 0.5 units/mL. Once the heparin solution was in the syringe, a 9-gauge needle with tubing was attached to the syringe for drawing blood from the donor.

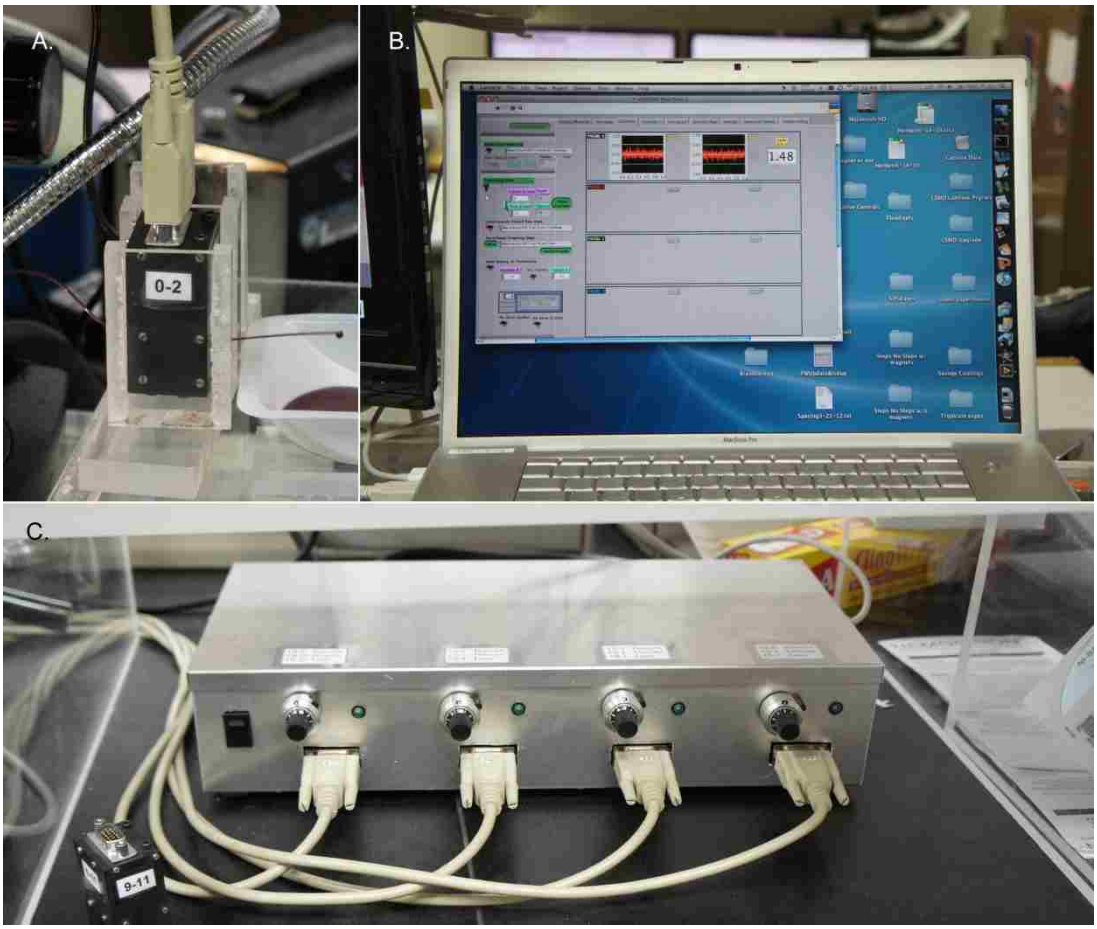

Figure 13: A) Laser Cuvette B) LabView® C) LSMD Controller.

After the draw, the blood in the syringe was mixed for a few minutes by pulling some air into the syringe and repeatedly rotating it 180^{o} in order to mix the heparin solution with the drawn blood. Then the air was pushed out, and the syringe was attached to the Luer head of the flow cell and placed on the syringe pump, ready for the experiment.

CHAPTER 5: EXPERIMENTAL DESIGN

5.1 Sample Selection

For this study, blood samples from a population of 33 donors (students from Brigham Young University) were initially tested for visibility of thrombus growth under the microscope. The variability of red cell content, platelet level, and other factors for each donor determine the reactivity and visibility of thrombus growth and embolization under the microscope. Therefore, an initial screening was conducted to identify donors that resulted in a high visibility of thromboembolism in the flow cell.

For the initial screening process, 33 volunteers who had not taken any medications for at least 2 weeks were brought in to test their blood response to the designed experiment. From each donor, 30 mL of blood were drawn, and the blood was pushed through the flow cell using the syringe pump under the following conditions: 1.0 mL/min flow rate, 0.5 units/mL heparin concentration, and 1.0 mm of space between two small tubes. At the end of the population screening, the blood samples from 8 donors were identified to have good visibility of thrombus growth under the microscope.

Each of the 8 donors was brought back on a weekly basis to complete a set of experiments to demonstrate that the developed method of studying thromboembolism can be used to evaluate the effects of controlled variables such as heparin concentration, flow rate, and the device design. The set of experiments is presented in Table 1.

Table 1: Experimental conditions

	Heparin concentration in blood	Blood Flow Rates	Spacing Between Two Small Tubes
Experiment 1	0.5 units/mL	1.0 mL/min	1.0 mm
Experiment 2	0.75 units/mL	1.0 mL/min	1.0 mm
Experiment 3	0.5 units/mL	0.5 mL/min	1.0 mm
Experiment 4	0.5 units/mL	1.0 mL/min	0.5 mm

The number of experiments required to develop the methodology combined with full factorial design resulted in a prohibitive-large number of experiments. Therefore, this simplified design was adopted where variables were tested one at a time against the baseline values. While this simplified design ignores variable-variable interactions, it still provides value in demonstrating that the developed method can be used to study the effects of controlled variables on thromboembolism.

5.2 The Effect of Heparin Concentration in Blood

Two sets of experiments were conducted at different levels of heparin concentration holding all other conditions the same. In Experiment 1, the heparin concentration level was set at 0.5 units of heparin per mL of blood, and in Experiment 2, the concentration was changed to 0.75 units of heparin per mL of blood. Higher concentrations of heparin (above 0.75 unit/mL of blood) yielded little to no visible thromboembolism under the microscope, while lower concentrations (below 0.5 unit/mL of blood) often resulted in a prohibitive amount of clotting in the apparatus.

5.3 The Effect of Blood Flow Rate

Two sets of experiments were conducted at different flow rates holding all other conditions the same. In Experiment 1, the flow rate of blood entering the flow cell was set at 1.0 mL/min (Re = 11.3), and in Experiment 3, the flow rate of blood entering the flow cell was lowered to 0.5 mL/min (Re = 5.65). Lower flow rates (lower than 0.5 mL/min) often did not result in visible thrombus growth under the microscope, and higher flow rates (greater than 1.0 mL/min) resulted in rapid embolization of thrombi, making it difficult to study thromboembolism in real-time.

The CFD results from *Star-CD® (CD-adapco)* showed that there is a significant difference in the velocity profiles for the two flow rates studied in this work. These CFD results are shown in Figure 14.

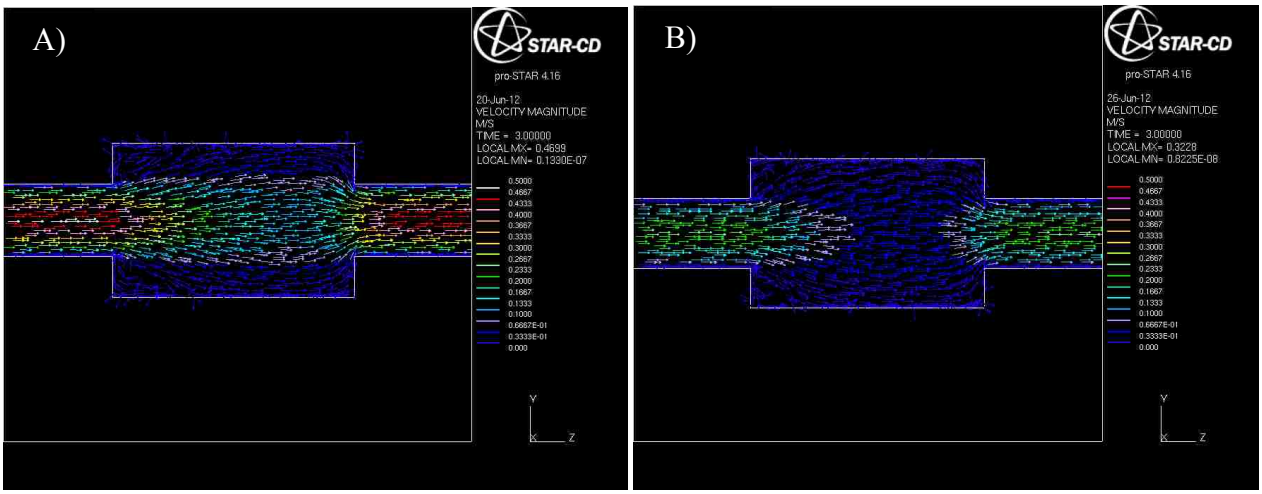

Figure 14: Velocity vector profile of A) 1.0 mL/min B) 0.5 mL/min.

5.4 The Effect of Device Design Change

The design of blood-contacting devices is one of the most important factors that controls thromboembolism in clinical settings, and is also one of the easiest variables to change to

minimize thromboembolism. To demonstrate that the developed method can be used to study the effects of device design change, two sets of experiments were conducted at different distances between two small tubes holding all other conditions the same. In Experiment 1, the distance between the two small tubes was 1.0 mm, and in Experiment 4, the distance between the two small tubes was 0.5 mm. The separation distances were determined after the CFD results from Star-CD® *(CD-adapco)* showed that the 1.0 mm distance between two inserts yielded flow reattachment at the wall prior to the second small tube, whereas the 0.5-mm distance between the small tubes yielded no reattachment of blood flow. These CFD results from *Star-CD® (CD-adapco)* are shown in Figure 15.

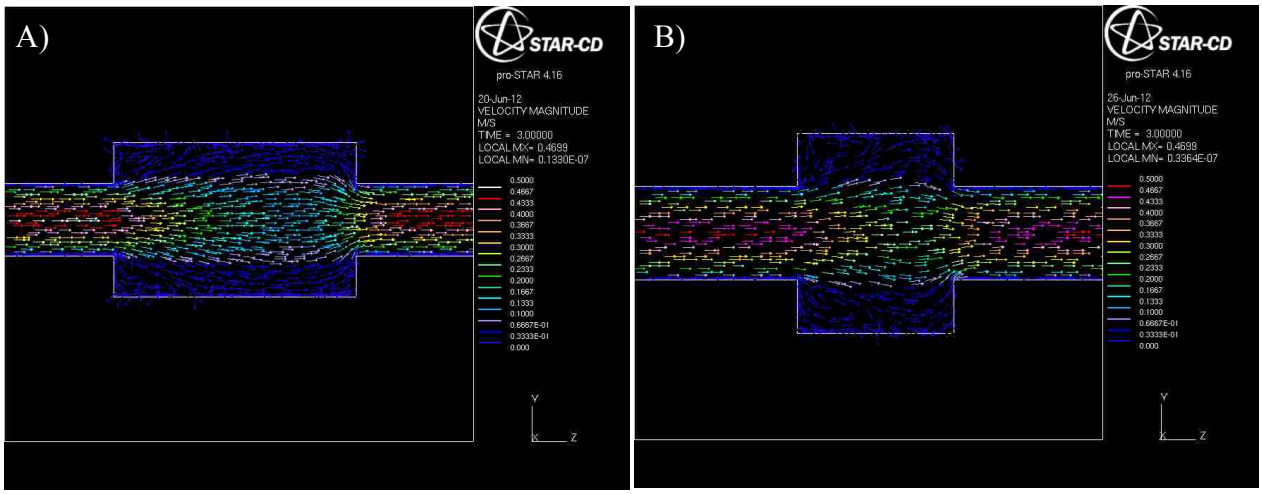

Figure 15: Velocity vector profile of A) 1.0 mm separation between two small tubes and B) 0.5 mm separation between two small tubes.

CHAPTER 6: CALCULATIONS OF THROMBOEMBOLISM PARAMETERS

After the high-definition videos of thromboembolism were acquired, the image-analysis software *ImageJ (National Institutes of Health)* was used to analyze the video for quantification of key thromboembolism parameters. Parameters of interest for this research included thrombus growth rate, thrombus growth direction, shear force on the thrombus, and adhesion strength of thrombus to the foreign surface.

An illustration of a thrombus in a flow cell, similar to the images captured using video microscopy for the current work, is shown in Figure 16.

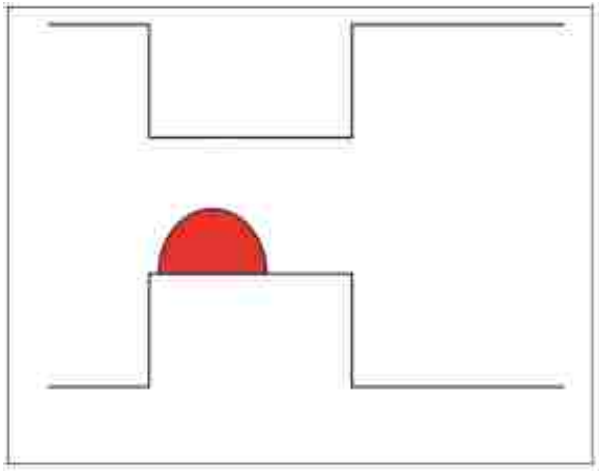

Figure 16: Illustration of thrombus growth in the flow cell.

Since the image captured in the video is two-dimensional, the cross sectional shape of the thrombus must be assumed. One logical assumption for the cross-sectional shape of the

thrombus is that it can be determined by the overlap of two circles with cross sections equal to that of the flow cell. The assumption of the cross-sectional shape of the thrombus used in the current work is represented in Figure 17. The height of the overlap is determined by the height of the thrombus as captured in the video microscopy images.

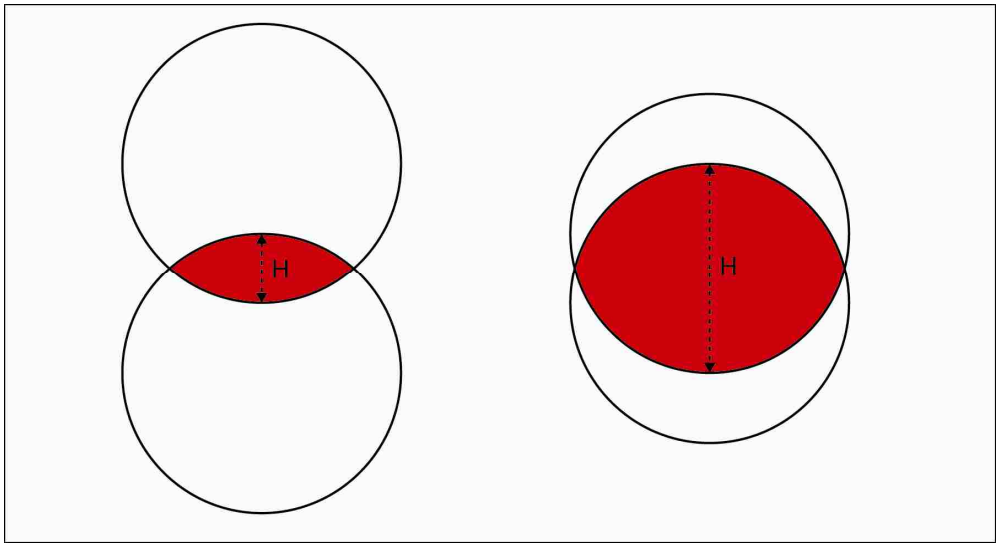

Figure 17: Assumed cross-sectional shape of the thrombus.

6.1 Calculation of Thrombus Growth Rate

In order to calculate the thrombus growth rate, the volume of the thrombus was estimated frame-by-frame from the two-dimensional image of the video microscopy. With the proposed assumption of the cross-sectional thrombus shape, the volume of the thrombus can be calculated using the following equation.

$$V_{thrombus} = \int_0^L A_{cs-thrombus} \cdot dx \tag{5}$$

As shown in Figure 18, the cross-sectional area of the thrombus can be determined by first calculating the half-height cross-sectional area (cross-hatched) and then multiplying that value by 2 ($A_{cs-thrombus} = 2 \cdot A_{cross-hatched}$).

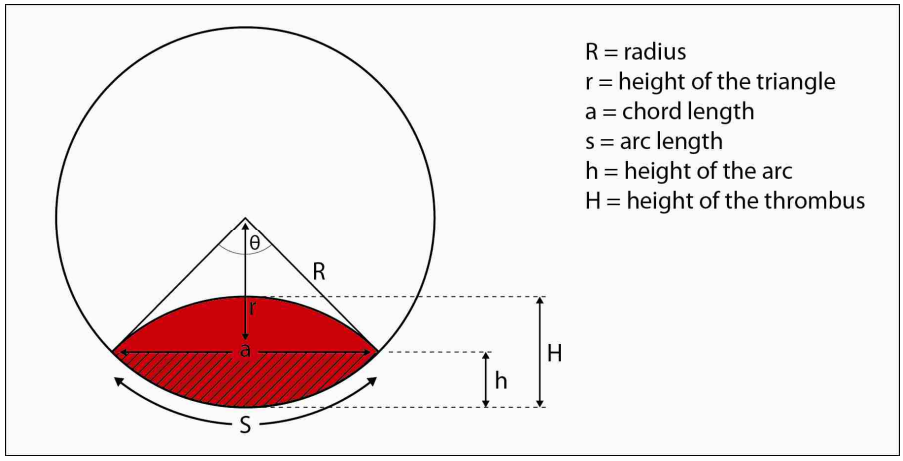

Figure 18: Terminology used in determination of thrombus area.

Using the terminology specified in Figure 18, the cross-sectional area of the thrombus was derived as shown.

$$H = 2 \cdot h \tag{6}$$

$$R = r + h \tag{7}$$

$$S = R \cdot \theta \tag{8}$$

$$\cos\left(\frac{1}{2}\theta\right) = \frac{r}{R} \tag{9}$$

$$R^2 = r^2 + (\frac{1}{2}a)^2 \tag{10}$$

$$\sin\left(\frac{1}{2}\theta\right) = {}^{\frac{1}{2}a}\Big/_{R} \tag{11}$$

Because $\mathrm{A}_{cross-hatched} = \mathrm{A}_{wedge} - \mathrm{A}_{triangle}$, $\mathrm{A}_{cross-hatched}$ was defined as:

$$\mathrm{A}_{cross-hatched} = \left(\frac{\theta}{2\cdot\pi} \cdot \pi \cdot R^2\right) - (\frac{1}{2} \cdot a \cdot r) \tag{12}$$

Using Eq. 8, Eq. 12 was further simplified to:

$$\mathrm{A}_{cross-hatched} = \left(\frac{1}{2} \cdot s \cdot R\right) - (\frac{1}{2} \cdot a \cdot r) \tag{13}$$

Using the relationships shown in Eq. 8, 9, and 10, Eq. 14 was derived for the cross-hatched section of the picture in Figure 18:

$$A_{cross-hatched} = \left(R^2 \cdot cos^{-1}\left(\frac{r}{R}\right)\right) - \left(r \cdot \sqrt{R^2 - r^2}\right) \quad (14)$$

Using Eq. 6 and 7, Eq. 14 was expressed in terms of height, H at any axial position, x:

$$A_{cross-hatched} = \left(R^2 \cdot cos^{-1}\left(\frac{R-\frac{1}{2}H(x)}{R}\right)\right) - \left(R - \frac{1}{2}H(x)\right) \cdot \left(\sqrt{R \cdot H(x) - \frac{1}{4}H(x)^2}\right) \quad (15)$$

$A_{cs-thrombus}$ is then $2 \cdot A_{cross-hatched}$, and

$$A_{cs-thrombus} = 2 \cdot \left(\left(R^2 \cdot cos^{-1}\left(\frac{R-\frac{1}{2}H(x)}{R}\right)\right) - \left(R - \frac{1}{2}H(x)\right) \cdot \left(\sqrt{R \cdot H(x) - \frac{1}{4}H(x)^2}\right)\right) \quad (16)$$

After integrating across the length of the thrombus, the approximate volume of the thrombus at any given time was calculated using Equation 17:

$$V_{thrombus} = \int_0^L 2 \cdot \left(\left(R^2 \cdot cos^{-1}\left(\frac{R-\frac{1}{2}H(x)}{R}\right)\right) - \left(R - \frac{1}{2}H(x)\right) \cdot \left(\sqrt{R \cdot H(x) - \frac{1}{4}H(x)^2}\right)\right) \cdot dx \quad (17)$$

Thrombus growth rate was estimated by using Equation 17 at each time frame of the experiment.

6.2 Calculation of Thrombus Growth Direction

The thrombus growth direction relative to the flow channel lumen was obtained by comparing the changes in the location of the thrombus center of mass at each time frame. The center of mass of the thrombus was determined from images taken from video microscopy using image software *Image J (National Institutes of Health)*. By plotting the position of the center of mass at successive times, the direction of the growth was determined.

6.3 Calculation of Shear Force on the Thrombus

As presented in Equation 2, shear force on the thrombus can be represented by

$$F = \sum (\tau \cdot A_s) \tag{18}$$

where A_s represents the surface area of the thrombus wetted by the flow of blood. Assuming the blood flow can be described by a one-dimensional Newtonian fluid, τ can be represented by Equation 19.

$$\tau = -\mu \cdot \frac{dv}{dl} \tag{19}$$

where μ represents the viscosity of the blood and $\frac{dv}{dl}$ represents the rate of change of fluid velocity with respect to the perpendicular distance from the thrombus surface. The shape of the blood flow cross section will change significantly as the thrombus grows, moving from a circle to a crescent as time passes. Therefore, the shear stress solution will need to adjust accordingly at various stages of thrombus growth, as shown in Figure 19.

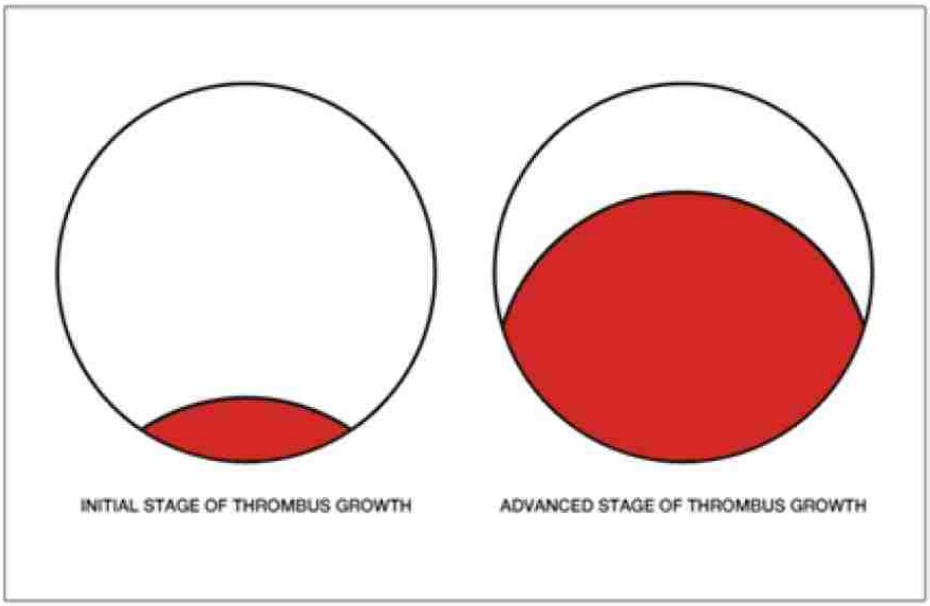

Figure 19: Illustration of thrombus growth stages.

6.3.1 Shear Stress Calculation at Initial Stages of Thrombus Growth

At the initial stages of thrombus growth, $\frac{\mathrm{H}}{R} \ll 1$, blood flow is similar to fully-developed laminar flow through a cylindrical pipe. The velocity profile of this solution can be approximated by Equation 20.

$$v = v_{\max}(1 - \frac{r^2}{R^2}) \tag{20}$$

where r is the radial position within the pipe. The velocity profile changes in the radial direction according to Equation 21.

$$\frac{dv}{dr} = \frac{-2\, r\, v_{\max}}{R^2} \tag{21}$$

For fully-developed laminar flow through a cylindrical pipe, $v_{\max} = 2\, v_{avg}$. Therefore, the shear stress across the surface of the thrombus at the initial stage, $\frac{\mathrm{H}}{R} \ll 1$, can be approximated by Equation 22.

$$\tau = -\mu \frac{dv_x}{dy} = \mu \frac{4\, r\, v_{\mathrm{avg}}}{R^2} \tag{22}$$

6.3.2 Shear Stress Calculation at Advanced Stages of Thrombus Growth

At the advanced stage of thrombus growth, which can be defined by $\frac{H}{R} > 1$, shear stress on the thrombus can be approximated by applying boundary-layer theory for flow between two flat plates. This is because the flow over the large thrombus creates a constantly-changing entrance region resulting in thin boundary layers at the surface but relatively-uniform velocity outside of the boundary layers (Figure 20).

The shear stress on the wetted surface of the thrombus can be estimated by the von Karman momentum balance [39] as shown in Equation 23.

$$\mu \frac{dv_x}{dy} = \frac{d}{dx}\int_0^\infty \rho v_x(v_e - v_x)dy + \frac{dv_e}{dx}\int_0^\infty \rho(v_e - v_x)dy \tag{23}$$

For this system, $v_e = v_\infty$. Assuming flow near the surface over the thrombus can be approximated by a flat-plate solution, the boundary-layer region can be sufficiently described by the velocity profile in Equation 24.

$$\frac{v_x}{v_\infty} = \frac{3}{2}\frac{y}{\delta} - \frac{1}{2}\left(\frac{y}{\delta}\right)^3 \tag{24}$$

where δ represents the boundary layer thickness shown in Figure 20. This profile has been defined such that $v_x = 0$ at $y = 0$ and $v_x = v_\infty$ at $y = \delta$. Because of the relatively-uniform velocities outside the boundary layers, v_∞ can be reasonably estimated to equal v_{avg}.

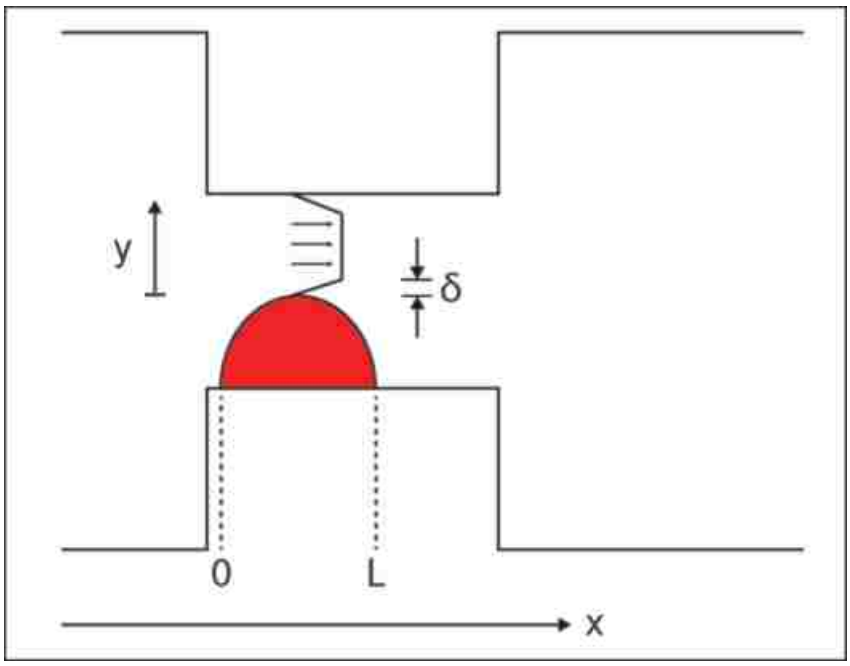

Figure 20: Representation of δ, L, y, x during thrombus growth in flow cell.

Substituting Equation 24 into the von Karman momentum balance and solving the differential equation results in Equation 25, which is a representation of the boundary-layer thickness of blood flow through a passage partially obstructed by the growing thrombus.

$$\delta(x) = \sqrt{\frac{280}{13}\frac{\vartheta x}{v_\infty}} = 4.64\sqrt{\frac{\vartheta x}{v_\infty}} \quad (25)$$

where ϑ is the kinematic viscosity and x is the distance from the leading edge of thrombus. Using Equations 24 and 25, we can calculate shear stress across the surface of the thrombus. This is given in Equation 26.

$$\tau = \mu\frac{dv_x}{dy} = \mu\frac{3v_\infty}{2\delta}\left(1 - \left(\frac{y}{\delta}\right)^2\right) \quad (26)$$

At the surface of the thrombus, $y = 0$, therefore Equation 26 reduces to:

$$\tau = \mu\frac{3v_\infty}{2\delta} \quad (27)$$

6.3.3 Shear Stress Calculation for Intermediate Stages of Thrombus Growth

As the thrombus grows from the initial stages, $\frac{H}{R} \ll 1$ to the advanced stages, $\frac{H}{R} \geq 1$, the solution for shear stress was described by a combination of the solutions for the initial and the advanced stages as shown in Equation 28.

$$\tau = \frac{R-H(x)}{R}\left(\mu\frac{4\,(R-H(x))\,v_{avg}}{R^2}\right) + \frac{H(x)}{R}\left(\mu\frac{3v_{avg}}{2\delta}\right) \quad (28)$$

where H(x) represents the thrombus height. Since advanced stage is defined by $\frac{H}{R} \geq 1$ and the initial stage is defined by $\frac{H}{R}$ close to 0, shear stress for an intermediate stage of thrombus growth, $\frac{H}{R} \leq 1$, was calculated using the ratio of height to radius.

6.3.4 Average Velocity Calculation

The average velocity, v_{avg}, was calculated using the volumetric flow rate of the blood and the cross-sectional flow area of the flow cell. Using Equation 6, the cross-sectional area of the blood flow was defined as:

$$A_{blood-flow} = (\pi \cdot R^2) - 2 \cdot \left(\left(R^2 \cdot cos^{-1} \left(\frac{R - \frac{1}{2}H(x)}{R} \right) \right) - \left(R - \frac{1}{2}H(x) \right) \cdot \left(\sqrt{R \cdot H(x) - \frac{1}{4}H(x)^2} \right) \right) \quad (29)$$

Using Eq. 29 and the known volumetric flow rate, an approximate v_{avg} for a given thrombus height was expressed as.

$$v_{avg} = \frac{Volumetric\ Flow\ Rate\ of\ Blood}{(\pi \cdot R^2) - 2 \cdot \left(\left(R^2 \cdot cos^{-1} \left(\frac{R - \frac{1}{2}H(x)}{R} \right) \right) - \left(R - \frac{1}{2}H(x) \right) \cdot \left(\sqrt{R \cdot H(x) - \frac{1}{4}H(x)^2} \right) \right)} \quad (30)$$

6.3.5 Calculation of Shear Force Acting on the Thrombus

The shear force on the surface of the thrombus (Equation 20) was calculated using the integral form shown in Eq. 31, where P is represented in Figure 21.

$$F = \int_0^L \tau(x) \cdot P(x) dx \quad (31)$$

In Figure 19, P(x) represents the top perimeter of the thrombus cross-section at any point x. P(x) was calculated by Equation 32.

$$P(x) = 2 \cdot R \cdot cos^{-1} \left(1 - \frac{H(x)}{2R} \right) \quad (32)$$

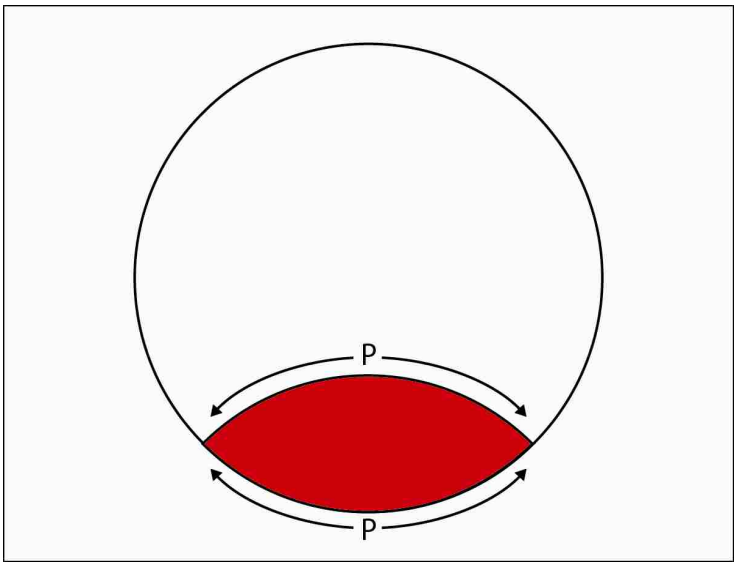

Figure 21: Illustration of the thrombus perimeter.

Combining Eq. 31 and 32, the shear force on the thrombus at any given time was estimated using Equation 33.

$$F = 2\int_0^L \tau(x) \cdot R \cdot cos^{-1}\left(1 - \frac{H(x)}{2R}\right) dx \quad (33)$$

H(x) was obtained by fitting the shape of the thrombus at a given time, and the integral in Equation 33 was then solved using numerical methods to determine the total shear force on the surface of the thrombus.

6.4 Calculation of Adhesion Strength of Thrombus

The thrombus embolizes when shear force on the thrombus exceeds the adhesion strength of the thrombus to the biomaterial. The adhesion strength was estimated by calculating the shear force at which the thrombus embolized and dividing it by the thrombus-biomaterial attachment area. The thrombus-biomaterial attachment area was calculated as shown in Equation 34.

$$A_{surface\text{-}bottom} = \int_0^L P(x)dx \quad (34)$$

Thus, adhesion strength of thrombus was calculated as shown in Equation 35.

$$S_{thrombus\text{-}adhesion} = \frac{F_{shear-embolization}}{A_{surface-bottom}} \quad (35)$$

CHAPTER 7: RESULTS AND DISCUSSION

Using the experimental design presented in Chapter 5, high-definition videos of thrombus formation and embolization in a miniature flow cell that mimics blood-contacting devices were acquired. The high-definition video was recorded at 29 frames-per-second, which gave the video a time resolution of 34.5 milliseconds. Therefore, any thromboembolism phenomena that occurred at time scales longer than 34.5 milliseconds were captured. This time resolution was deemed sufficient after viewing the first few acquired videos and noting that the pertinent phenomena of thrombus growth were being captured. An example of the still frames taken from the captured videos of thromboembolism is shown in Figure 22.

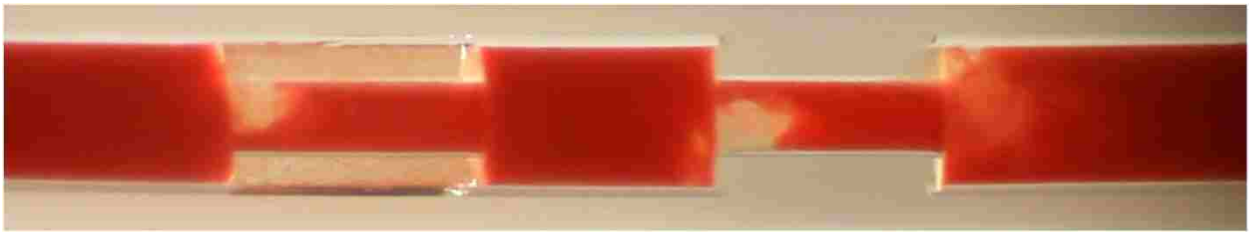

Figure 22: An example of a still frame taken from the captured video of thrombus growth in the flow cell.

The actual process of embolization was also captured in some of the videos. However, capturing embolization proved to be more difficult than anticipated due to how quickly the embolization occurred. This will be discussed further in Section 7.2.

All data collected as part of this research and reported in this chapter will be presented as means with 95% confidence intervals. The significance of differences were evaluated with

Pearson's chi-squared test and Student's t-test. The results from the two statistical tests were in agreement. In this work, statistical significance is presented with p-values from the Student's t-test.

7.1 Thrombus Formation

The experimental techniques used for this research were well-suited to studying thrombus formation and growth. Initial thrombus formation and steady thrombus growth were visible under the microscope for long periods of time. Using the high-definition videos acquired, the location of thrombus growth, thrombus growth rate, thrombus growth direction, and shear force on the surface of the thrombus were each evaluated. Additionally, the effects of flow rate, heparin concentration in blood, and small-tube spacing on these thrombus growth parameters were explored. The 37 high-definition videos acquired showed a total of 129 growing thrombi, of which 45 were analyzed and presented in this chapter.

7.1.1 Thrombus Growth Location

All 129 thrombi observed in this study grew in one of two locations within the flow cell. These two locations are shown in Figure 23.

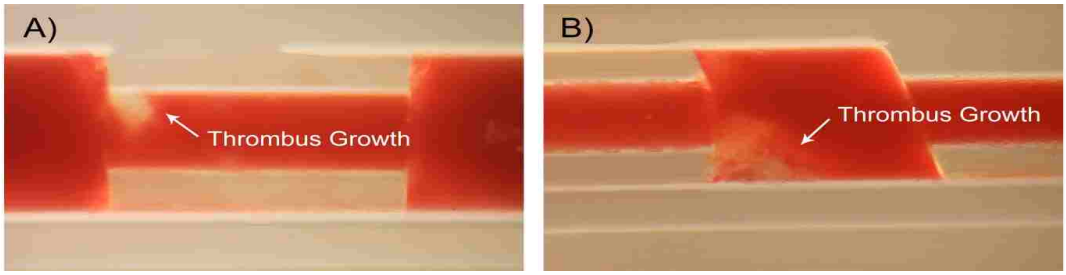

Figure 23: Common locations of thrombus growth within the flow cell the small tube entrance and B) at the large tube following the small tube exit.

The location of thrombus growth shown in Figure 23A was at the entrance of a small tube. Out of the 129 thrombi seen through the microscope, 61 (47%) were seen at this location. The remainder of the visible thrombi, 68 (53%), grew in the large tubes immediately following the small tube exit, as shown in Figure 23B.

The location of common thrombus growth within the large tubes can be explained by the presence of a recirculation zone at that location. Blood in recirculation zones experiences an increased residence time, which allows for longer exposure of flowing platelets and thrombogenic agents in the blood to foreign surfaces and to existing thrombi [27].

Thrombus growth at the leading edge of the small tube is more difficult to explain. Initially, it was believed that the constricted flow and sharp edge at the entrance of the small tube caused the activation of platelets, and thus thrombi began to grow at that location. However, further visual analysis showed that the thrombi may begin to grow within the recirculation zone in the large tube just prior to the small tube entrance, and then spread up into the restricted flow area in the small tube as they grow.

In most of the acquired videos, this phenomenon was difficult to observe due to the limited transparency of blood in the large tubes. In a few cases, this phenomenon was captured, and an example is shown in Figure 24.

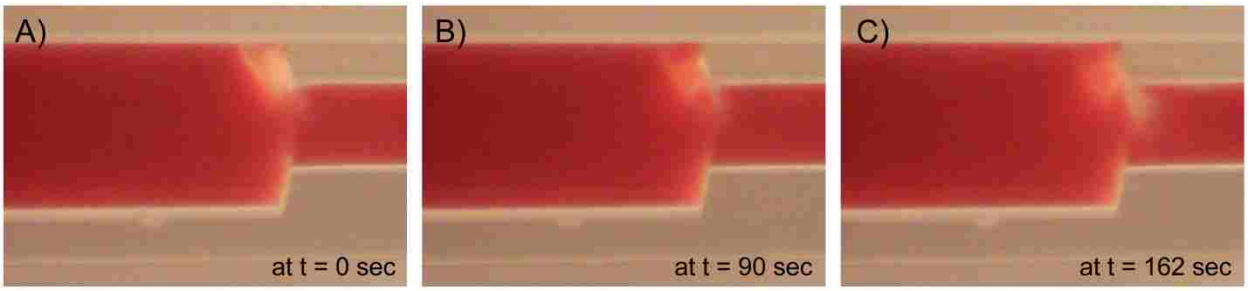

Figure 24: Thrombus growth from large tube into small A) t = 0 B) t = 1:30 C) t = 2:42.

In a perfect flow cell with cylindrical symmetry, the thrombus might be expected to form uniformly around the inside of the tube at each axial location. However, experimental observations show that thrombi form at random angular positions around the insides of the small and the large tubes. This non-uniformity is probably due to inconsistencies and imperfections of the flow cells. Although significant effort was put into making a well-built flow cell, the cut faces of the inserts and the fit of the inserts against the tubing wall were seen to be irregular when viewed under the microscope, which may have caused the variations of thrombus angular growth location that were observed.

7.1.2 Thrombus Growth Rate

As discussed previously, steady thrombus growth was visible under the microscope in real-time. An example of thrombus growth obtained is shown in Figure 25.

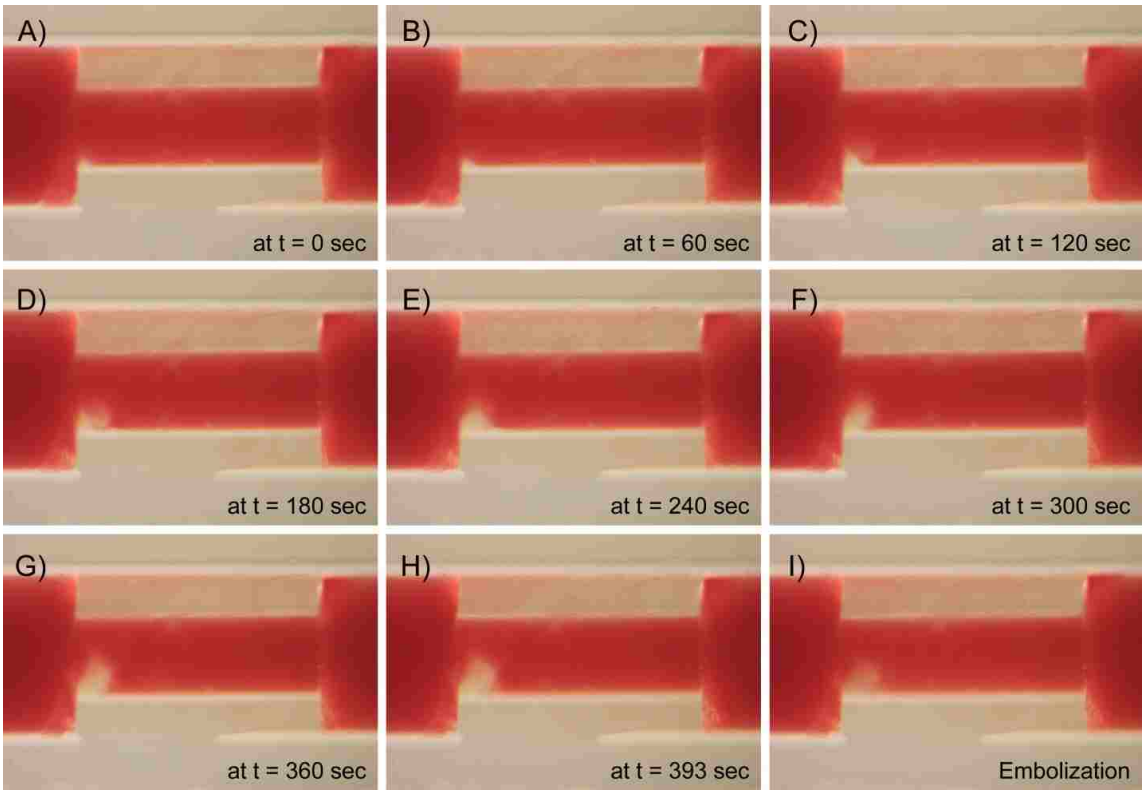

Figure 25: High-definition images of thrombus growth.

From the 129 thrombi observed, 45 thrombi were analyzed. The high-definition video was first imported into *Image J (National Institutes of Health)*, which took individual still frames from the video at specified time intervals. These images were analyzed by *Image* J, which returned height vs. axial position data for the outer boundary of a visible thrombus. An example of the *Image J* output is shown in Appendix A. For most video analyses, 30 second intervals were used. An example of the conversion from video image to plotted boundary is shown in Figure 26.

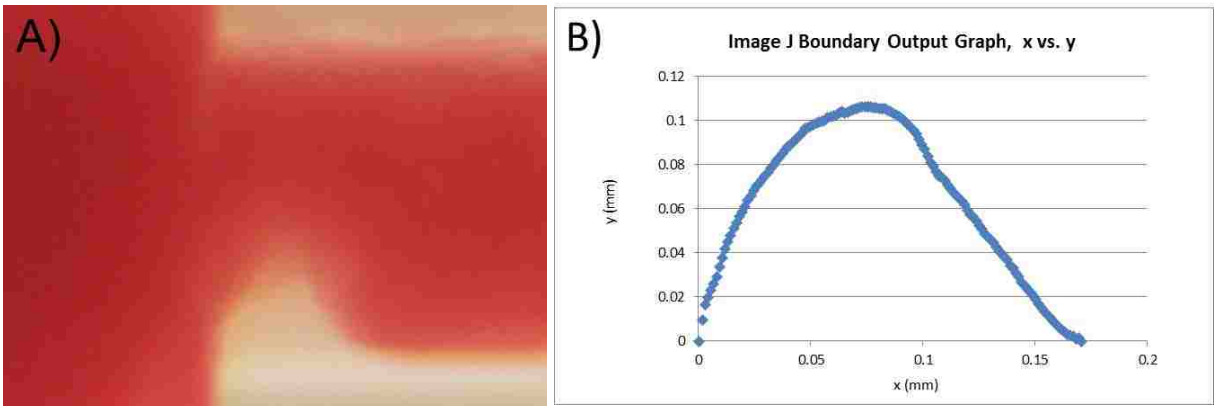

Figure 26: Comparison of A) video image to B) plotted boundary from *Image J* output.

An equation was fit to the graphical boundary data (Figure 26B), which represented the height of the thrombus at any axial position at a given point in time. This equation was applied to the calculation presented in Section 6 to determine the volume of the thrombus at that time. An example of this calculation is shown in Appendix B. After estimating the thrombus volume at each of the specified times, a plot of thrombus volume vs. time was constructed.

Of the 45 thrombi analyzed, 32 contained data beginning early in the thrombus growth process, and only these were used for thrombus growth evaluation (19 in the small tubes and 13 in the large tubes). An evaluation of thrombus volume vs. time showed that thrombus growth in the small and large tubes followed separate patterns. Of the 19 thrombi in the small tubes that

were analyzed, 17 showed a growth pattern similar to that of a power-law relationship as a function of time. Twelve of the 13 thrombi in the large tubes that were analyzed showed a growth pattern similar to that of linear growth. Examples of the small and the large tube thrombus growth patterns are shown in Figure 27.

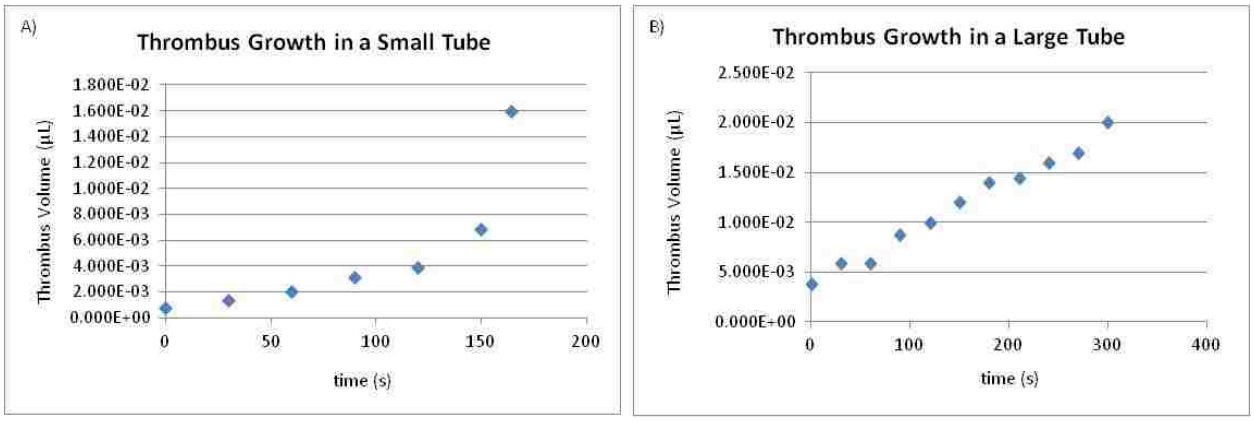

Figure 27: Thrombus volume vs. time A) in a small tube and B) in a large tube.

The difference in thrombus growth patterns between the small and large tubes can be explained by analyzing the methods of transport of blood components to existing thrombi. As shown in Figure 14, the location where thrombus growth occurs in the small tubes has a relatively high flow velocity and is likely dominated by the convection of blood components to an existing thrombus. (The Sherwood number for a tube without a thrombus is reported to be 3.66 [40]).

As a thrombus grows in the small tube, the flow becomes more constricted and the velocity increases, which leads to an increase in the convective transport of blood components to the thrombus. The Sherwood number of an entry region for laminar flow that is not fully developed can be approximated by the following correlation [40].

$$\overline{\mathrm{Sh}_D} = 1.86 \left(\frac{Re_D Sc}{\frac{L}{D}} \right)^{\frac{1}{3}} \left(\frac{\mu}{\mu_s}\right)^{0.14} \tag{36}$$

For the experimental conditions in the study where the temperature is constant, the viscosity ratio reduces to 1. As the velocity increases due to a growing thrombus, the Reynolds number in Equation 36 will increase, which leads to an increase in the Sherwood number. This implies that the effects of the convective transport of blood components to an existing thrombus have increased.

In the large tubes, the velocity surrounding the growing thrombus is near-zero (Figure 14), and therefore, the associated Reynolds number will be close to 0 and the Sherwood number will be close to 1. This Sherwood number approximation reflects that the transport of blood components to the thrombus in the large tubes is dominated by diffusion. As the thrombus volume increases in this location, the flow profile around the growing thrombus is not altered significantly, and therefore there is no impact on thrombus growth rate.

An increase in the velocity of blood flow due to a growing thrombus in the small tubes will also increase the shear stress related to blood flow. This raises a question of whether shear-related platelet activation can occur [41]. The estimated range of shear stress for the experimental conditions in this study is 100 to 500 dynes/cm^2 and the estimated range for the exposure time is 0.1 to 5 milliseconds. An example of this estimation is shown in Appendix C. According to the criteria proposed by Hellums, this range of shear stress and exposure time is well below the threshold for activation of platelets by shear stress [41], and thus, there should not be an effect on thrombus growth due to platelet activation caused by an increase in shear stress.

The thrombus growth rate in the large and small tubes were compared by plotting thrombus growth rate with respect to time, as shown in Figure 28. The magnitude of change in the thrombus growth rate (increase or decrease) was determined by evaluating the slope of thrombus growth rate over time.

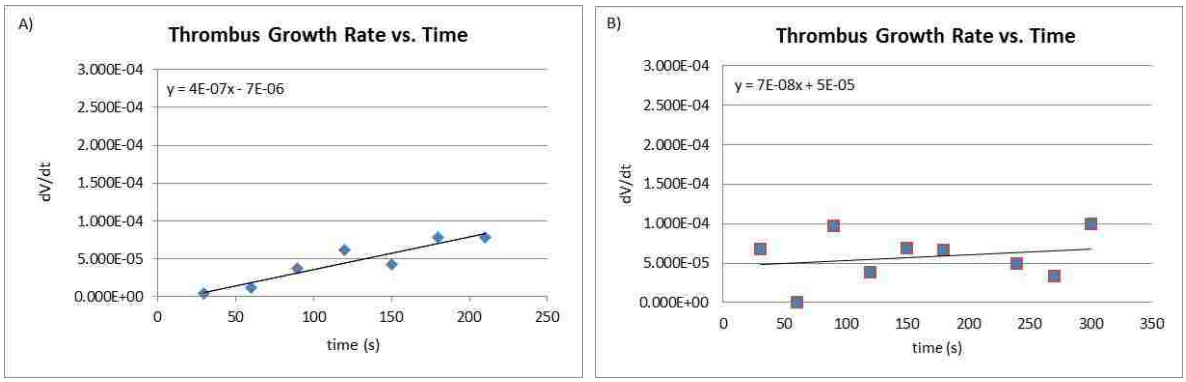

Figure 28: An example of thrombus growth rate vs. time in A) small tubes and B) large tubes.

The average slopes of thrombus growth rate with respect to time for thrombi in small tubes (n =19) and that for large tubes (n=13) are presented in Table 2. The slope of thrombus growth rate in the small tubes was significantly greater than that of the large tubes. Such a large difference in the slope of thrombus growth over time between the small and the large tubes is consistent with the idea of convection domination in the small tubes and the diffusion domination in the large tubes as discussed earlier.

Table 2: Slope of thrombus growth rate with respect to time

	Slope of Thrombus Growth Rate (mL/s^2)
Small Tubes (n = 19)	5.72E-07 ± 2.64E-07 (95% confidence)
Large Tubes (n = 13)	1.34E-07 ± 6.08E-08 (95% confidence)
p-value	0.013

Effect of Heparin Concentration on Thrombus Growth Rate

As discussed in Section 2.4, one possible effect of an increase in heparin concentration in the blood is a decrease in thrombus formation by inhibiting the participation of fibrin, thus decreasing thrombus growth rate. The results in Table 3 showed that no such effect was present; however, due to the small number of data points, there was no significant difference either way.

When evaluating paired differences within donors, results varied widely and the differences were not statistically significant.

Table 3: Effect of heparin concentration on slope of thrombus growth rate over time

Small Tubes	**Mean ± 95% conf. interval (mL/s^2)**
Heparin Concentration = 0.5 units/mL (n = 6)	6.25E-07 ± 5.53E-07
Heparin Concentration = 0.75 units/mL (n = 4)	8.25E-07 ± 8.63E-07
p-value	0.697
Large Tubes	**Mean ± 95% conf. interval (mL/s^2)**
Heparin Concentration = 0.5 units/mL (n = 2)	1.50E-07 ± 9.80E-08
Heparin Concentration = 0.75 units/mL (n = 2)	2.50E-07 ± 9.80E-08
p-value	0.293

Effect of Flow Rate on Thrombus Growth Rate

A decrease in blood flow rate can lead to a decrease in the convective transport of platelets and other blood components to an existing thrombus, which would decrease thrombus growth rate. However, a decrease in blood flow rate can also lead to an increase in residence time of blood around the existing thrombus, which would increase thrombus growth rate. The results from Table 4 suggest a decrease in the slope of thrombus growth rate with decreasing flow rate in both the small and large tubes. However, the results were not statistically significant, even when individual donors were evaluated.

Table 4: Effect of flow rate on the slope of thrombus growth rate over time

Small Tubes	**Mean ± 95% conf. interval (mL/s^2)**
Flow Rate = 1.0 mL/min (n = 6)	6.25E-07 ± 5.53E-07
Flow Rate = 0.5 mL/min (n = 5)	3.24E-07 ± 2.68E-07
p-value	0.393
Large Tubes	**Mean ± 95% conf. interval (mL/s^2)**
Flow Rate = 1.0 mL/min (n = 2)	1.50E-07 ± 9.80E-08
Flow Rate = 0.5 mL/min (n = 1)	7.00E-08
p-value	N/A

Effect of Device Design on Thrombus Growth Rate

An experiment was conducted to demonstrate an application of the developed method to study the effect of change in device design on the thrombus growth rate. As discussed previously in Section 5, the spacing between the two small tubes was decreased from 1 mm to 0.5 mm. As this change in device design only affects the flow pattern of the blood at locations between two successive small tubes, only thrombus data from these locations were analyzed. From the 45 thrombi analyzed, 8 (2 from the baseline experiment and 6 from the decreased-spacing experiment) qualified for this study.

A decrease in the spacing between two successive small tubes resulted in a flow pattern where the main flow stream does not re-attach to the surface of the large tube following the expansion created at the end of a small tube. This created a larger recirculation zone at the surface. Assuming that the growth mechanism for thrombi in this location is diffusion controlled, one possible result of this change in device design would be a decrease in the slope of thrombus growth rate because the diffusion distance from the main flow stream to the existing thrombus has increased due to no flow reattachment to the surface. The results suggest that a decrease in the spacing between two successive small tubes leads to a significant decrease in slope of thrombus growth rate (Table 5).

Table 5: Effect of device design on the slope of thrombus growth rate over time

Large Middle Tubes	Mean ± 95% conf. interval (mL/s^2)
Spacing = 1 mm (n = 2)	1.50E-07 ± 9.80E-08
Spacing = 0.5 mm (n = 6)	6.17E-08 ± 2.60E-08
p-value	0.039

7.1.3 Thrombus Growth Direction

Thrombus growth direction was estimated by tracking the thrombus center of mass with respect to time. The output from *Image J* for center of mass was given in Cartesian coordinates with the origin located at the upstream edge of the thrombus adjacent to the biomaterial surface. The assumption made in this approximation is that the three-dimensional shape of the thrombus can be sufficiently represented by a two-dimensional image. An example of the center of mass changing with respect to time, using Cartesian coordinates in two dimensions, is shown in Figure 29.

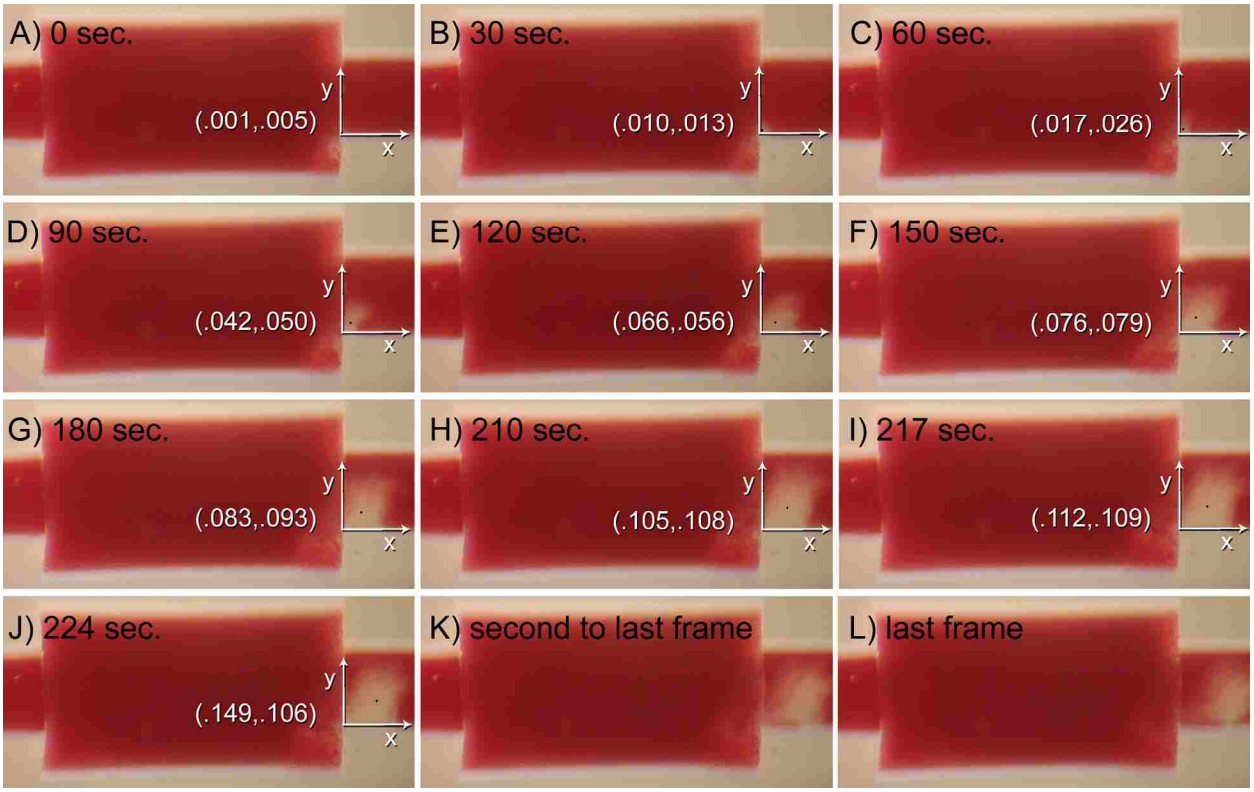

Figure 29: Change in thrombus center of mass with respect to time.

Of the 45 thrombi analyzed, 29 were used for this study. The remaining 16 were rejected due to one of two reasons: 1) thrombus growth was not captured during the early stages of growth and 2) thrombus growth was captured from an angle that was not comparable to other

videos. After the center of mass data were collected, they were graphed in Cartesian coordinates to determine the direction of thrombus growth. An example of this is shown in Figure 30.

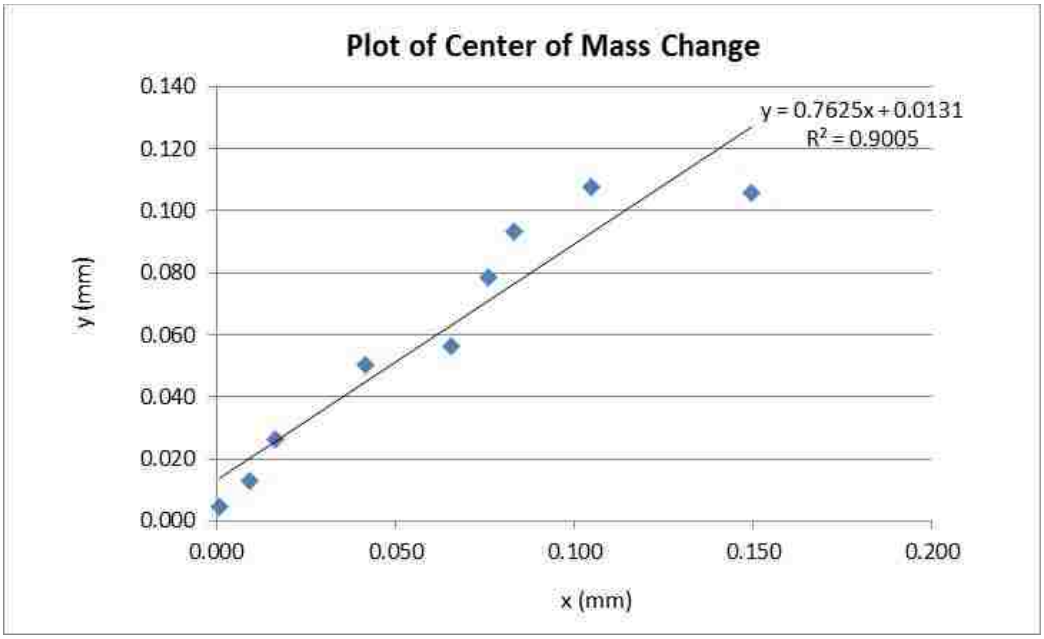

Figure 30: An example of the thrombus center of mass change, in Cartesian coordinates.

To quantify the direction of the center of mass change, and thus direction of thrombus growth, an equation was fit to the data with the trendline function in Excel *(Microsoft®)*. The best fit to the data was determined to be a straight line and the slope of that line was used to calculate the thrombus growth direction angle, which typically ranged from 15 to 35 degrees. Thrombus growth angles for the large and small tubes were not significantly different (Table 6).

Table 6: Thrombus growth direction in the small and large tubes

	Thrombus Growth Direction (degrees)
Small Tubes (n = 18)	25.78 ± 5.22 (95% confidence)
Large Tubes (n = 11)	23.59 ± 12.96 (95% confidence)
p-value	0.637

Effect of Heparin Concentration on Thrombus Growth Direction

One possible effect of heparin concentration on thrombus growth direction might be that it affects the mechanical strength of the developing thrombus. An increase in heparin concentration in blood could lead to a decrease in mechanical strength of thrombi due to a decrease in fibrin participation during thrombus growth. Thus, it is possible that the developed thrombus at higher heparin concentration could deform more easily as blood flow tends to push the thrombus downstream. However, no such effect is suggested by the data (Table 7).

Table 7: Effects of heparin concentration in blood in thrombus growth direction

Small Tubes	**Mean ± 95% conf. interval (degrees)**
Heparin Concentration = 0.5 units/mL (n = 6)	27.66 ± 9.29
Heparin Concentration = 0.75 units/mL (n = 5)	25.48 ± 2.79
p-value	0.696
Large Tubes	**Mean ± 95% conf. interval (degrees)**
Heparin Concentration = 0.5 units/mL (n = 3)	25.27 ± 13.91
Heparin Concentration = 0.75 units/mL (n = 2)	22.03 ± 24.79
p-value	0.821

Effect of Flow Rate on Thrombus Growth Direction

A decrease in flow rate can lead to an increase in thrombus growth direction because less force is pushing the thrombus downstream. However, the results show no significant difference in thrombus growth direction in either the small or large tubes (Table 8).

Table 8: Effect of flow rate on the thrombus growth direction

Small Tubes	**Mean ± 95% conf. interval (degrees)**
Flow Rate = 1.0 mL/min (n = 6)	27.66 ± 9.29
Flow Rate = 0.5 mL/min (n = 3)	32.47 ± 21.45
p-value	0.644
Large Tubes	**Mean ± 95% conf. interval (degrees)**
Flow Rate = 1.0 mL/min (n = 3)	25.27 ± 13.91
Flow Rate = 0.5 mL/min (n = 1)	23.12 ± 14.16
p-value	N/A

Effect of Device Design on Thrombus Growth Direction

As described in Section 7.1.2, only results from the thrombi that grew in the large tube between two successive small tubes were considered. As the velocity at the location where the thrombus grows in the large tubes is near zero for both cases, this device design change should lead to no effect on thrombus growth direction, consistent with results presented in Table 9.

Table 9: Effect of device design on thrombus growth direction

Large Middle Tubes	Mean ± 95% conf. int. (degrees)
Spacing = 1 mm (n = 3)	25.27 ± 13.91
Spacing = 0.5 mm (n = 5)	23.12 ± 14.16
p-value	0.851

7.1.4 Shear Force Acting on the Thrombus

Shear force on observed thrombi was estimated according to the calculations shown in Chapter 6. As discussed in Section 7.2, a thrombus boundary equation was obtained from *Image J* at specified times. This thrombus boundary equation was then used as an input for calculating shear force on the thrombus. A sample of the shear force calculation is shown in Appendix C. A plot of the calculated shear force on a thrombus with respect to time is shown in Figure 31.

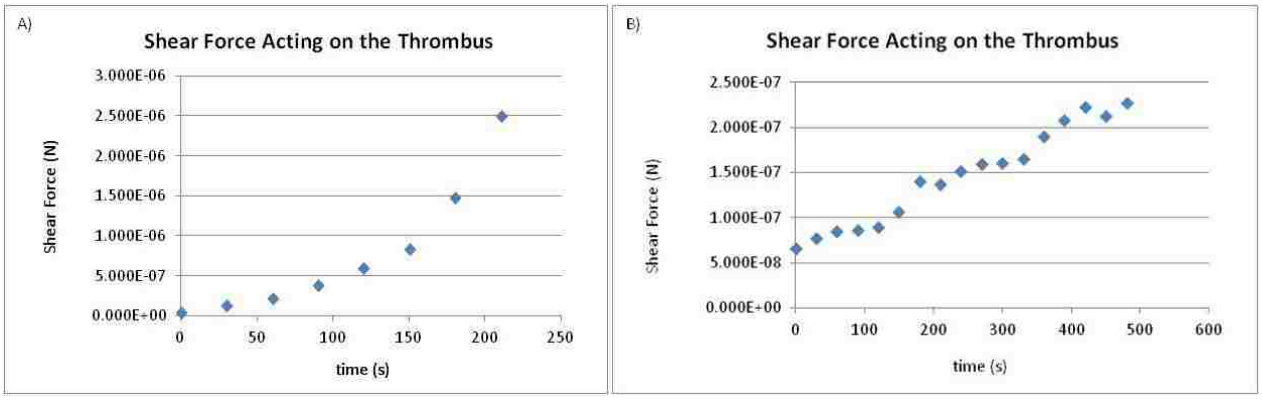

Figure 31: An example of shear force acting on a thrombus with respect to time for A) small tubes B) large tubes.

For each thrombus growth observed, the shear force acting on it was calculated at specified time intervals (in most cases 30 seconds) to analyze how the shear force changed as the thrombus grew.

The pattern of shear force acting on the thrombus with respect to time mirrored the pattern of thrombus volume change. For thrombi in the small tubes, the shear force acting on the thrombus increased as a power-law-like function of time. For thrombi in the large tubes, the shear force acting on the thrombus increased as a linear-like function of time. As the factors that determine the shear force acting on the thrombus (mainly the blood flow velocity and the surface area of the thrombus) depend on the size of the thrombus, it seems logical that the pattern of shear force acting on the thrombus with respect to time would follow that of thrombus volume growth.

7.2 Embolization

The mechanism of embolization is difficult to determine due to the limited temporal and spatial resolution of the current experimental techniques. Embolization occurred so quickly that it was difficult to capture the detail necessary to determine the mechanism. However, after observing the several high-definition videos acquired, the following two mechanisms can be proposed:

1) Complete detachment of a thrombus from the foreign surface
2) Partial embolization of a thrombus by internal tearing

The first mechanism is shown in Figure 32 where the entire thrombus stays intact and seems to slide down the surface before embolizing.

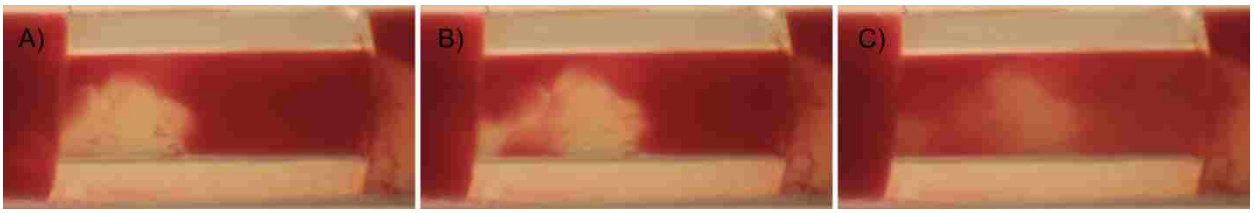

Figure 32: Thrombus sliding along the surface of the biomaterial surface before embolizing.

Alternatively, partial embolization can sometimes occur by internal tearing of the thrombus due to the shear forces acting on the thrombus. Although the partial embolization of a thrombus was very difficult to observe in detail, a few of the videos acquired showed a change in shape of thrombus which proved that the partial embolization can occur.

7.2.1 Calculation of Shear Force Acting on the Thrombus at Embolization

From the 45 thrombi analyzed, 19 thrombi that grew in the small tubes and 4 thrombi that grew in the large tubes embolized. Of the 19 thrombi that embolized in the small tubes, 3 were rejected because visual observation showed that they either embolized due to impact from an embolus released at an upstream location or because an attachment (another thrombus) to the thrombus was visible at embolization but not during thrombus growth.

Comparing the 16 embolization events from the small tubes and 4 from the large tubes showed that the shear force at which the thrombus embolized was significantly higher for thrombi in the small tubes (Table 10).

Table 10: Shear force acting on the thrombus at embolization

	Shear Force at Embolization (N)
Small Tubes (n = 16)	1.79E-06 ± 5.05E-07 (95% confidence)
Large Tubes (n = 4)	3.49E-07 ± 3.42E-07 (95% confidence)
p-value	0.014

The higher shear force acting on the thrombus at embolization for thrombi in the small tubes can be explained in two possible ways. First, thrombi in the large tubes were embolizing due to factors other than just the shear force acting on the thrombus, such as being impacted by emboli released at an upstream location. All 4 videos of large-tube embolization had thrombi that were large enough to protrude into the upstream emboli path, and one of the 4 videos available actually showed an embolization event associated with a collision from an upstream embolus.

Another possible explanation is that the thrombi that grow in the small tubes may be a different type of thrombus than those that grow in the large tubes, and therefore they embolize at a different shear force threshold. The high-flow velocity in the small tubes might prevent red cells from being captured by the thrombus, which would result in the development of what is often referred to as a white thrombus. In the large tubes, low-flow velocity results in many red cells becoming part of the thrombus and forming what is often referred to as a red thrombus [42]. However, due to the presence of heparin, which inhibits fibrin formation, thrombi that grow in the large tubes are not the typical red thrombus that includes fibrin; rather they are more like white platelet thrombi that also captured some red blood cells. This was consistent with experimental observations wherein thrombi that formed in the small tubes appeared more solidly white than thrombi that grew in the large tubes, which were more red in color (see Figure 23).

In an analysis of the effect of controlled variables on the shear force at embolization, only 4 of the 21 analyzed thrombi in the large tubes embolized, thus not enough data were collected to report any results for embolization in the large tubes. For thrombi in the small tubes, both an increase in heparin concentration and a decrease in flow rate resulted in shear forces at the time of embolization that were not statistically different from the baseline experiments (Table 11).

Table 11: Effect of heparin concentration and flow rate on the shear force at embolization

	Mean ± 95% conf. int. (N)	p-value
Hep. Conc. = 0.5 units/mL, Flow Rate = 1 mL/min (n=8)	1.89E-06 ± 8.59E-07	
Hep. Conc. = 0.75 units/mL, Flow Rate = 1 mL/min (n=3)	2.04E-06 ± 1.48E-06	0.861
Hep. Conc. = 0.5 units/mL, Flow Rate = 0.5 mL/min (n=2)	1.93E-06 ± 2.86E-07	0.966

7.2.2 Adhesion Strength

The hypothesis describing embolization is that it occurs when the shear force on a thrombus exceeds the adhesion strength between the thrombus and the foreign surface. Associated with this hypothesis is the expectation that the estimated shear force per estimated thrombus-biomaterial attachment area ($F_{shear}/A_{attached}$) would start out less than some critical value during early development of the thrombus and would increase to that critical value as the thrombus grows, at which time, embolization would occur. In fact, the evaluation of $F_{shear}/A_{attached}$ in a few representative thrombi demonstrated that pattern (Figure 32).

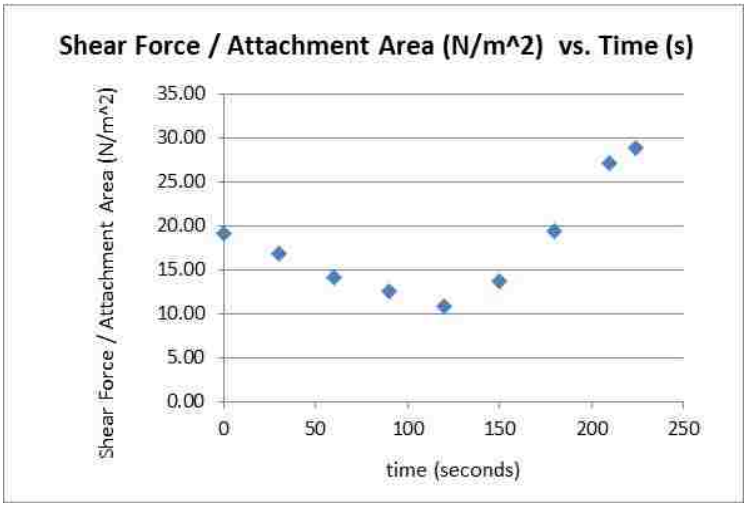

Figure 33: Shear force acting on a thrombus divided by assumed thrombus attachment area.

Figure 33 shows that for one of the thrombi examined, $F_{shear}/A_{attached}$ initially decreased but as the thrombus grew, this ratio began to increase until the threshold limit for embolization

was exceeded. The decrease of $F_{shear}/A_{attached}$ in the initial phase was unexpected, and could be a real phenomenon or be occurring as a result of the assumptions made about the thrombus shape (Chapter 6).

The adhesion strength of a thrombus to a foreign surface was estimated using the estimated shear force at the time of embolization and dividing it by the estimated thrombus-biomaterial attachment area. An example of this calculation is shown in Appendix D. As with the calculation of shear force at the time of embolization, only 16 thrombi from the small tubes were analyzed. The results of adhesion strength of thrombi are presented in Table 12.

Table 12: Thrombus adhesion strength in the small and large tubes

	Adhesion Strength (N/m^2)
Small Tubes (n=16)	16.24 ± 2.59 (95% confidence)

The adhesion strength for thrombi in the small tubes ranged from 9.63 to 28.83 N/m^2 with an mean value of 16.24 ± 2.59 N/m^2 (95% confidence). This result is remarkably close to the results published by Goodman [43] for the removal of platelets by various values of shear stress using radiolabeling and scanning electron microscopy. From Goodman's data, 70 - 90% removal of platelets occurred at shear stresses of 13 - 25 N/m^2.

The effects of changes in heparin concentration and flow rate on the adhesion strength of thrombi in the small tubes were analyzed (Table 13). The results suggest that neither a change in heparin concentration nor flow rate had a statistically significant effect on thrombus adhesion strength.

Table 13: Effect of heparin concentration and flow rate on the adhesion strength

	Ave. ± 95% conf. int. (N/m^2)	p-value
Hep. Conc. = 0.5 units/mL, Flow Rate = 1 mL/min (n=8)	17.40 ± 4.36	
Hep. Conc. = 0.75 units/mL, Flow Rate = 1 mL/min (n=3)	18.18 ± 4.23	0.846
Hep. Conc. = 0.5 units/mL, Flow Rate = 0.5 mL/min (n=2)	14.96 ± 4.12	0.619

7.2.3 Light-Scattering Microemboli Detector Output Analysis

The light-scattering microemboli detector (LSMD) detected the number and size of emboli passing through the flow cell by differentiating the light-scattering patterns created by emboli from patterns created by the red blood cells and other blood components [37]. The LSMD reports four separate streams of data with respect to time. These outputs include:

1) Instantaneous peak: detection of a single embolus or single group of emboli
2) Cumulative peak: sum of all emboli that have passed the detector from time = 0
3) Instantaneous moment: length scale (diameter) of the detected embolus or group of emboli
4) Cumulative moment: sum of instantaneous moments from time = 0

Although the cumulative peak count of thrombi data is important, the most informative of these outputs is the cumulative moment because it represents the sum of emboli diameters that were detected throughout the entire experiment.

In the study of the effects of "controlled variables" (heparin concentration, flow rate, and device design), the cumulative peak count and cumulative moment were also recorded by the LSMD. Since the LSMD detects many more emboli than could be tracked by videomicroscopy, sufficient data were available to use a paired-difference analysis. Because the response of blood to the experimental conditions varies from donor to donor and even from day to day for the same donor, this kind of paired-difference analysis minimizes the effects of donor and day-to-day variations and focuses more directly on the variable of interest. Thus for each donor on each day,

the difference was computed between the cumulative peak count for the conditions of altered controlled variable (e.g. increased heparin concentration, etc.) versus for the baseline conditions. A similar difference was computed for the cumulative moment. The means of those paired differences were evaluated against the null value of zero using the Student t-test (see Table 14).

Table 14: The means of cumulative peak count and cumulative moment

	Mean of Cumulative Peak Count % Change ± 95% Confidence Interval	p-values	Mean of Cumulative Moment % Change ± 95% Confidence Interval	p-values
Increase in Heparin Concentration (from 0.5 units/mL to 0.75 units/mL) (n = 7)	-37.82% ± 25.59%	0.013	-42.47% ± 19.53%	0.001
Decrease in Flow Rate (from 1 mL/min to 0.5 mL/min) (n = 3)	-24.93% ± 59.53%	0.458	-71.32% ± 36.90%	0.019
Decrease in Spacing between Tubes (from 1 mm to 0.5 mm) (n = 5)	17.79% ± 58.55%	0.568	21.50% ± 38.74%	0.308

An increase in heparin concentration of blood led to a 38% decrease in the cumulative peak count and a 42% decrease in the cumulative moment. These results are in agreement with the notion that an increase in the heparin concentration in the blood decreases the fibrin participation in thrombus formation and thus decreases the formation of emboli large enough to be seen by the LSMD. A decrease in flow rate resulted in a significant decrease in the cumulative moment; however the cumulative peak count difference was insignificant. Also, a decrease in the spacing between the two small tubes (inserts) resulted in no significant difference both cumulative peak count and cumulative moment.

7.3 Comparison of Experimental Results to Andersen CFD Model

Andersen developed a real-time three-dimensional CFD model for predicting thrombus formation and embolization in blood-contacting devices [44]. As part of the current research,

experimental results were compared to this CFD model results under the same conditions as those used in our experiments.

The thrombus growth locations predicted by the Andersen CFD model for the same conditions used in this research are shown in Figures 34 and 35. Figure 34 is a prediction of thrombus formation in the flow cell at t = 1044. Figure 35 represents the fraction of time occupied by thrombi throughout an entire 1200-second simulation. Color variations represent the fractions of time that each location was a thrombus.

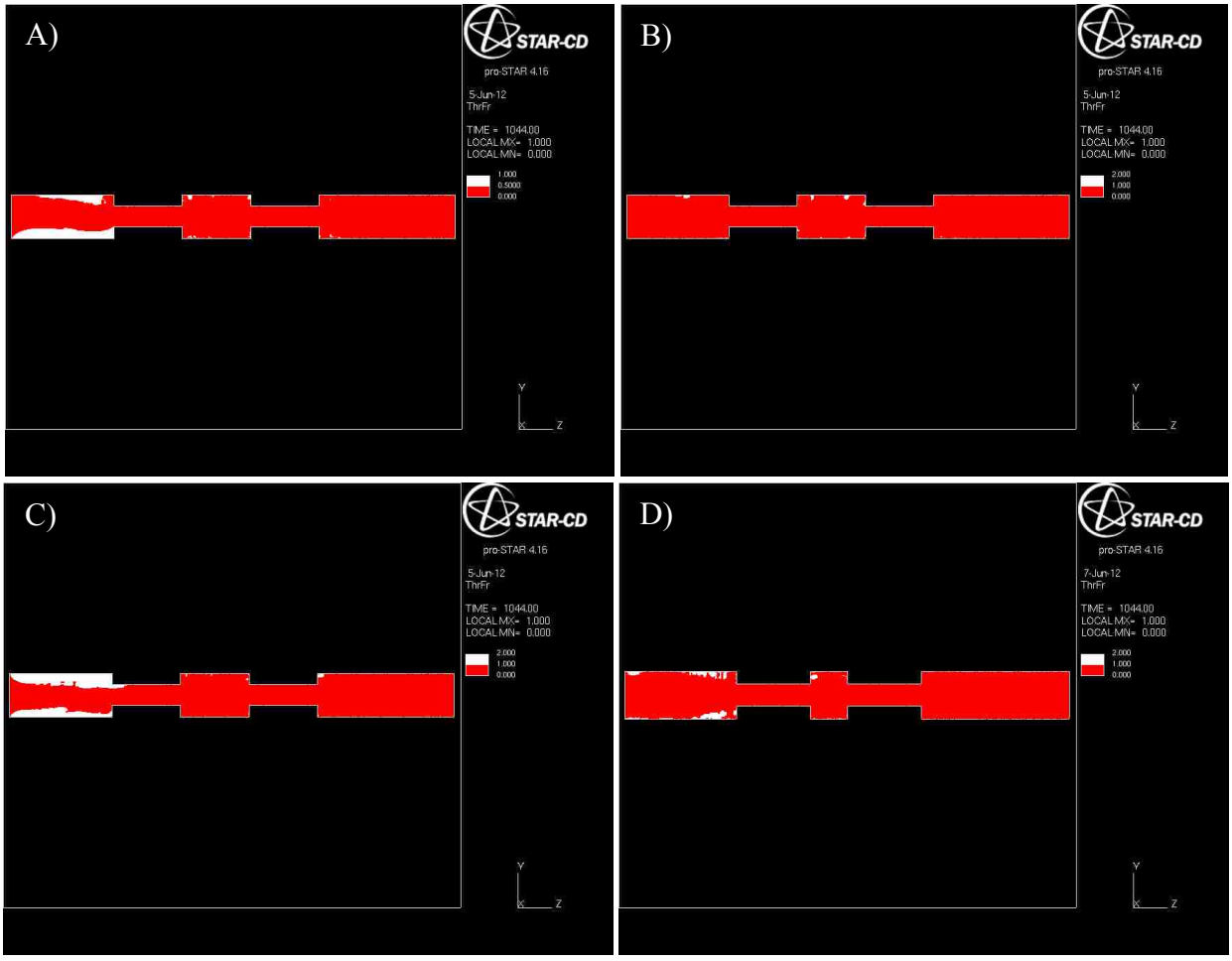

Figure 34: Thromboembolism predictions from Andersen CFD model at t = 1044 seconds A) experiment 1 B) experiment 2 C) experiment 3 and D) experiment 4 [see Table 1].

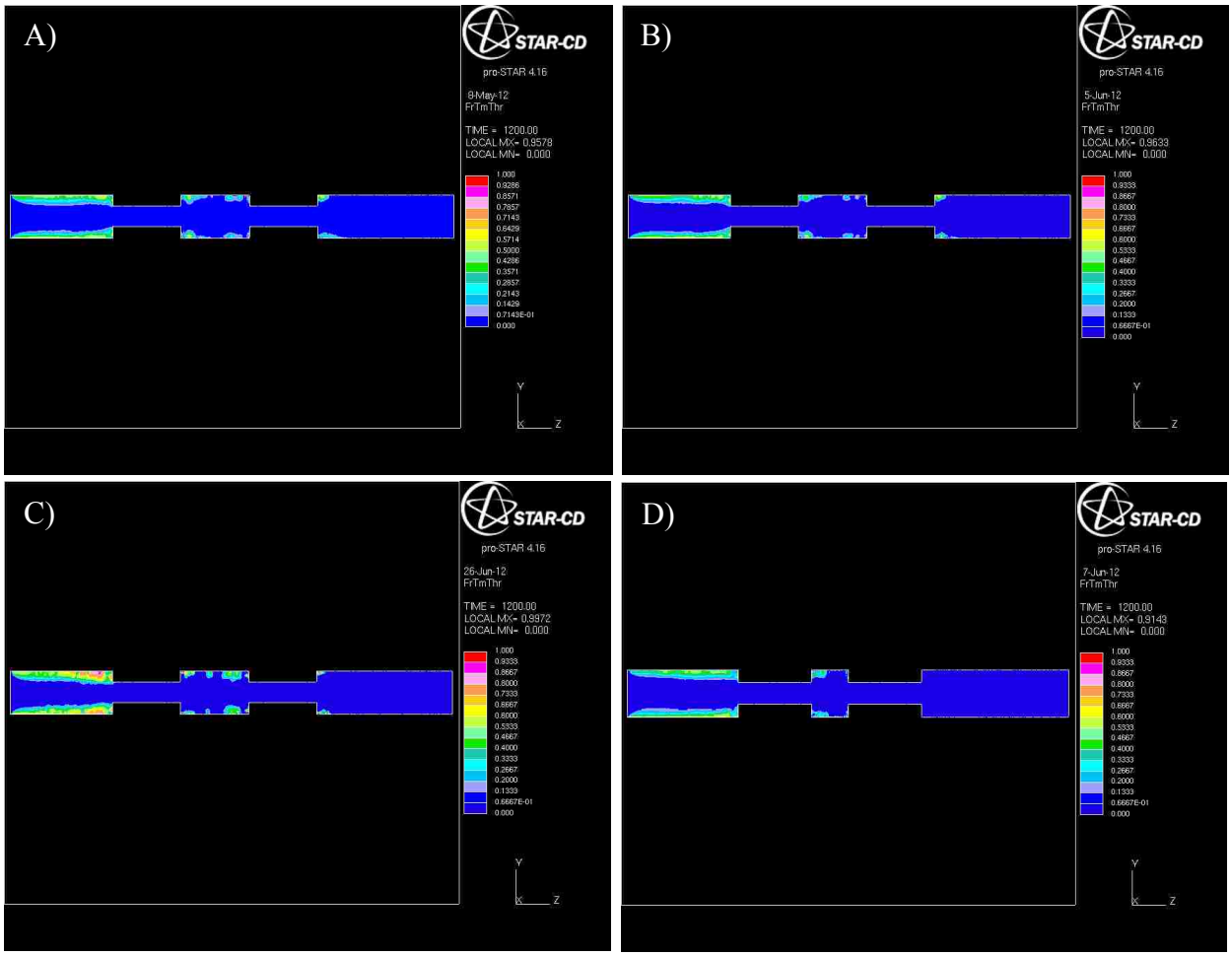

Figure 35: Fraction of time occupied by a thrombus for 1200 second simulations A) experiment 1 B) experiment 2 C) experiment 3 and D) experiment 4 [see Table 1].

For the most part, the CFD model predictions for thrombus growth locations disagreed with observations from current experimental study. The CFD model predicts that most of the thrombus growth exists upstream of the small-tube inserts near the entrance region of the flow cell. Experimental observations from the current research show that most thrombus growth occurs just upstream or just downstream of the small tubes. Also according to experimental observation, thrombi often grow at the leading edge of the small tubes, which is not reflected in the CFD model predictions.

The mean cumulative emboli counts of 8 donors for each of the experimental conditions at t = 1200 seconds are presented and compared to CFD predicted emboli counts at t = 1200 seconds (Table 15).

Table 15: Mean paired differences for cumulative peak count and cumulative moment (altered conditions minus baseline conditions). P-values reflect the probability of the differences equaling zero.

	Experiment Emboli Count at t=1200s ± 95% Conf. Interval	p-value	CFD Predicted Emboli Count at t = 1200s
Baseline Experiment (n = 7)	244.14 ± 169.87		22210
Increase in Heparin Concentration (from 0.5 to 0.75 units/ml) (n = 7)	164.43 ± 91.44	0.434	21860
Decrease in Flow Rate (from 1 mL/min to 0.5 mL/min) (n = 4)	160.00 ± 122.87	0.574	20352
Decrease in Spacing between Small Tubes (from 1 mm to 0.5 mm) (n = 6)	203.10 ± 111.30	0.731	16081

The CFD-predicted emboli count was about two orders of magnitude higher than the mean experimental count. However, the vast majority of emboli predicted by the CFD model are in the 20-30 micron range, which is much smaller than the detection limit of the LSMD. Therefore, a direct comparison between experimental emboli count and the CFD model prediction cannot be made.

CHAPTER 8: SUMMARY AND CONCLUSIONS

In this work, a unique and novel method to study thromboembolism by direct observation was developed. High-definition videos of thrombus formation and embolization in miniature flow cells that mimic blood-contacting devices using in-vitro, non-invasive, real-time techniques were successfully obtained. The obtained videos were analyzed using the image-analysis software, *Image J (National Institutes of Health)* to determine critical parameters of thromboembolism such as thrombus growth rate, thrombus growth direction, shear force acting on the thrombus with respect to time, shear force on the thrombus at embolization, and adhesion strength of the thrombus to the foreign surface. Also, characteristics of thrombus growth location and embolization were observed and reported.

For the flow cell used, the thrombus growth was found in predominantly two locations. Thrombi grew in the flow recirculation zone just after the trailing edge of the small tubes 53% of the time. For the remaining 47% of the time, thrombi grew at the leading edge of the small tubes. However, several thrombus growth video observations suggest that at least some, if not all, thrombus formation in the small tubes actually starts in the flow recirculation zone just before the leading edge of the small tubes and then spreads into the small tubes. It can be concluded from these results that flow recirculation zones play a major role in initial thrombus formation.

After estimating the thrombus volume and shear force acting on the thrombus at specified times, patterns of thrombus growth for small and large tubes were identified. In the small tubes, thrombus volume and shear force acting on the thrombus showed a growth pattern that behaved

like a power-law function of time. In the large tubes, thrombus volume and shear force acting on the thrombus showed a growth pattern that was like a linear function of time. The difference in patterns of thrombus growth and shear force acting on the thrombus between the small and large tubes was explained by the methods of transport of blood components. The location where thrombus growth occurred in the small tubes had a high flow velocity and is likely to be dominated by the convection of blood components to an existing thrombus; however, the recirculation zone in the large tubes that promotes thrombus growth has near-zero velocity, and thus the transport of blood components to an existing thrombus is dominated by diffusion.

The average slopes of thrombus growth rate with respect to time for thrombi in small tubes and that for large tubes were determined. The slope of thrombus growth rate in the small tubes was significantly greater than that in the large tubes. The thrombus growth direction was determined by tracking the thrombus center of mass with respect to time. To quantify the direction of the center of mass change, and thus direction of thrombus growth, a straight line was fit to the data and the slope of that line was used to calculate the thrombus growth direction angle, which typically ranged from 15 to 35 degrees from the direction of flow. The difference between thrombus growth angles for the large and small tubes was insignificant.

According to a frame-by-frame observation of embolization videos, embolization seems to occur via two possible mechanisms: complete detachment of the thrombus by sliding off the foreign surface or partial embolization of the thrombus by internal tearing. The difference of shear force on the thrombus at the time of embolization between the small and the large tubes were significant. The shear force at embolization in the small tubes was 1.79E-06 ± 5.05E-07 (95% confidence) and that in the large tubes was 3.49E-07 ± 3.42E-07 (95% confidence). The difference in shear force at the time of embolization in the small and the large tubes was

explained by two possible ways. First, thrombi in the large tubes were embolizing due to factors other than just the shear force acting on the thrombus, such as a result of being impacted by emboli from upstream. Second, the thrombi that grow in the small tubes could be a different type of thrombus than those that grow in the large tubes, and therefore they embolize at a different shear force threshold.

The adhesion strength of a thrombus was calculated for the small tubes using the shear force at embolization and the estimated thrombus attachment area. The calculated adhesion strength ranged from 9.63 N/m^2 to 28.83 N/m^2 with a mean of 16.24 ± 2.59 (95% confidence). This result is remarkably close to the results published by Goodman [43] for the removal of platelets by various values of shear stress using radiolabeling and scanning electron microscopy. From Goodman's data, 70 - 90% removal of platelets occurred at shear stresses of 13 - 25 N/m^2.

Next, the developed method was used to demonstrate that the effects of controlled variables such as heparin concentration in blood, blood flow rate, and the device design on thromboembolism could be studied. The changes in controlled variables were:

- Heparin concentration in blood - 0.5 units/mL vs. 0.75 units/mL
- Blood flow rate - 0.5 mL/min vs. 1.0 mL/min
- Spacing between two successive small tubes within the flow cell - 0.5 mm vs. 1.0 mm

The controlled variables were tested one at a time against the baseline experiment results of critical thromboembolism parameters. Also, paired differences within donors of cumulative peak count of thrombi and the cumulative moment of thrombi from LSMD output was compared.

Due to the small sample size used in this research, the results from the changes in controlled variables were statistically insignificant. However, the results suggest that with larger number of experiments and full factorial experimental design that include variable-variable

interactions, the developed method can be used to study the effects of controlled variables on thromboembolism.

Lastly, the observation and data collected from the experiments in this research were compared to the predictions of a CFD model developed by Andersen [44] under identical conditions. For the most part, the CFD model predictions for the thrombus growth locations disagreed with experimental observations. The emboli count comparison couldn't be directly made because the vast majority of emboli predicted by the CFD model are in the 20-30 micron range, which is much smaller than the detection limit of LSMD. However, both models did show the importance of flow recirculation zones for thromboembolism activity and similar trends for changes in three controlled variables.

CHAPTER 9: FUTURE DIRECTION

While current experimental techniques for capturing the details of thromboembolism under a microscope performed sufficiently well for this work, significant improvements can be made in the experimental setup and methods employed to obtain results that would be both more consistent and more accurate.

The most significant improvements that can be made to the experimental setup would be to acquire a higher-quality microscope and high-definition camera. A microscope with better optics and a high-definition camera with a higher recording frame rate would allow for a better visual image of thrombus growth, but more importantly, would be able to capture embolization events in higher detail. Also, with an improved video recording system, rather than focusing only on one part of the flow cell, the entire flow cell could be observed with the same or better quality image of thrombus growth and embolization.

Although it may be very difficult to achieve, developing a three-dimensional camera system that could observe thrombus growth from all angles surrounding the flow cell would significantly improve the quality of results. The largest assumption made by the current research was to approximate the three-dimensional thrombus shape with an acquired two-dimensional image.

Video recordings of thrombus growth for initial experiments conducted in the current research began once thrombus formation was observed. This frequently resulted in a lack of data during the initial stages of thrombus growth. A better method of recording would have been to

start the recording process immediately after blood entered the flow cell. Also, using a parallel means of analysis for testing the effects of all controlled variables on thromboembolism would be ideal because blood from a single donor can respond differently on a day-to-day basis.

Lastly, increasing the pool of donors and number of experiments while using a full factorial design of controlled variables would help to increase the confidence in the experimental results.

REFERENCES

1. Bittl, J.A., *Coronary stent occlusion: thrombus horribilis*. J. Am. Coll. Cardiol., 1996. **28**(2): p. 368-70.

2. Bick R.L., *Hemostasis defects associated with cardiac surgery, prosthetic devices, and other extracorporeal circuits*. Semin. Thromb. Hemost., 1985. **11**(3): p. 249-80.

3. Clagett G.P. and R.C. Eberhart, *Artificial devices in clinical practice*, in *Hemostasis and Thrombosis: Basic Principles and Clinical Practice*, 3rd edition, R.W. Colman, J. Hirsh, V.J. Marder and E.W. Salzman, Editors. 1996, J. B. Lippincott Company: Philadelphia. p. 1486-505.

4. Turitto, V.T. and H.R. Baumgartner, *Platelet-surface interactions,* in *Hemostasis and Thrombosis: Basic Principles and Clinical Practice,* 2nd Edition*,* R.W. Colman, J. Hirsh, V.J. Marder, and E.W Salzman, Editors. 1987, J. B. Lippincott Company: Philadelphia. p. 555-571.

5. Zhao, X and J.M. Courtney, *Surface modification of biomaterials by heparinisation to improve blood compatibility*, in *Surface Modification of Biomaterials; Methods, Analysis and Applications*, R. Williams, Editors. 2011, Woodhead Publishing Limited: Cambridge. p. 55-77.

6. Petschek, H., D. Adamis and A.R. Kantrowitz, *Stagnation Flow Thrombus Formation*. Trans. Am. Soc. Artif. Intern. Organs, 1968. **14**(1): p. 256-60.

7. Goodman P.D., M.W. Hall, S. Sukavaneshvar and K.A. Solen, *In Vitro Model for Studying the effects of hemodynamics on device induced thromboembolism in human blood*, American Society of Artificial Internal Organs, 2000. **46**(5): p. 576-8.

8. Vasiliev, J.M. and I.M. Gelfand, *Mechanism of non-adhesiveness of endothelial and epithelial surfaces*, Nature, 1978. **274**(5672): p. 710-1.

9. Colman, R.W., V.J. Marder, E.W. Salzman and J. Hirsh, *Overview of hemostasis,* in *Hemostasis and Thrombosis: Basic Principles and Clinical Practice,* 2nd Edition*,* R.W. Colman, J. Hirsh, V.J. Marder, and E.W Salzman, Editors. 1987, J. B. Lippincott Company: Philadelpha, p. 3-17.

10. Weiss, H.J. and V.T. Turitto, *Prostacyclin (Prostaglandin I_2, PGI_2) inhibits platelet adhesion and thrombus formation on subendothelium*. Blood, 1979. **53**(2): p. 244-50.

11. Hatton, M.W.C., L.R. Berry and E. Ragoeczl, *Inhibition of thrombin by antithrombin III in the presence of certain glycosaminoglycans found in the mammalian aorta*. Thrombosis Research, 1978. **13**(4): p. 655-70.

12. Teien, A.N., U. Abildgaard and M. Hook, *The anticoagulant effect of heparin sulfate and dermatan sulfate*. Thrombosis Research, 1976. **8**(6): p. 859-69.

13. Esmon, C.T. and W.G. Owen, *Identification of an endothelial cell cofactor for thrombin-catalyzed activation of protein C.* Proc. Natl. Acad. Sci. USA, 1981. **78**(4): p. 2249-2252.

14. Pasi, K.J., *Hemostasis: components and processes*, D.J. Perry and K.J. Pasi, Editors. 1999, Humana Press Inc: New Jersey. p. 3-21.

15. Turitto, V.T., H.J. Weiss, H.R. Baumgartner, *The effect of shear rate on platelet interaction with subendothelium exposed to citrated human blood*. Microvascular Research, 1980. **19**(3): p. 352-365.

16. Adams, G.A., S.J. Brown, L.V. McIntire, S.G. Eskin and R.R. Martin, *Kinetics of platelet adhesion and thrombus growth*. Blood, 1983. **62**(1): p. 69-74.

17. Hammarstrom, S., J.A. Lindgren and P. Roos, *Biosyntheses of prostaglandins and thromboxanes* in *Chemistry, Biochemistry and Pharmacological Activity of Prostanoids*, S.M. RoberTs and F. Scheinmann, Editors. 1979, Pergamon Press Ltd: New York. p. 221-232.

18. Vroman, L., *The life of an artificial device in contact with blood: initial eventas and their effect on its final state*. Bull NY Acad Med, 1988. **64**(4): 352-357.

19. Andrade, J.D. and V. Hlady, *Protein adsorption and material biocompatibility: A tutorial review and suggested hypotheses*. Adv Polym Sci, 1986. **79**: 1-63.

20. Brash, J.L., *Role of plasma protein adsorption in the response of blood to foreign surfaces*, in *Blood Compatible Materials and Devices*, C.P. Sharma and M. Szycher, Editors. 1991, Technomic Publishing Company, Inc: Pennsylvania. p. 3-19.

21. Gorbet, M.B. and M.V. Sefton, *Biomaterial-associated thrombosis: roles of coagulation factors, complement, platelets and leukocytes*. Biomaterials, 2004. **25**(26): 5681-703.

22. Kroll, M.H., J.D. Hellums, L.V. McIntire, A.I. Schafer and J.L. Moake, *Platelets and shear stress*. Blood, 1996. **88**(5): p. 1525-41.

23. Turitto, V.T., A.M. Benis and E.F. Leonard, *Platelet diffusion in flowing blood*. Ind. Eng. Chem. Fundam., 1972. **11**(2): p. 216-223.

24. Grabowski, E.F., L.I. Friedman and E.F. Leonard, *Effects of shear rate on the diffusion and adhesion of blood platelets to a foreign surface*. Ind. Eng. Chem. Fundam., 1972. **11**(2): p. 224-232.

25. Lever, M.J., *Mass transport processes in artificial organs,* in *Biomaterials, Artificial Organs and Tissue Engineering*, L.L. Hench and J.R. Jones, Editors. 2005, Woodhead Publishing Limited: Cambridge. p. 153-66.

26. Cooney, D.O., *Biomedical Engineering Principles, An Introduction to Fluid, Heat, and Mass Transport Processes*. 2nd Edition. 1976, New York: Marcel Dekker, Inc. 458.

27. Hubbel, J.A. and L.V. McIntire, *Platelet active concentration profiles near growing thrombi*. Biophys J., 1986. **50**(5): p. 937-45.

28. Bernstein, E.F., P.L. Blackshear Jr and K.H. Keller, *Factors influencing erythrocyte destruction in artificial organs*. The American Journal of Surgery, 1967. **114**(1): p. 126-38.

29. Brown C.H., L.B. Leverett, C.W. Lewis, C.P. Alfrey and J.D. Hellums, *Morphological, biochemical, and functional changes in human platelets subjected to shear stress*. J. Lab. Clin. Med, 1975. **86**(3): p. 462-71.

30. Anderson, G.H., J.D. Hellums, J. Moake and C.P. Alfrey, *Platelet response to shear stress: changes in serotonin uptake, serotonin release, and ADP induced aggregation*. Thrombosis Research, 1978. **13**(6): p. 1039-47.

31. O'Brien J.R., *Shear-induced platelet aggregation*. Lancet, 1990. **335**(8691): p. 711-3.

32. Lever, M.J., *Artificial exchange systems,* in *Biomaterials, Artificial Organs and Tissue Engineering*, L.L. Hench and J.R. Jones, Editors. 2005, Woodhead Publishing Limited: Cambridge. p. 169-72.

33. Hirsh J., R. Raschke, T.E. Warkentin, J.E. Dalen, D. Deykin and L. Poller, *Heparin: mechanism of action, pharmacokinetics, dosing considerations, monitoring, efficacy, and safety*. Chest, 1995. **108**(4): p. 258S-75S.

34. Adams, G.A., L.V. McIntire, R.R. Martin, J.D. Olson and H. Sybers, *The effects of heparin and polymorphonuclear neutrophil leukocytes on platelet aggregate formation on collagen-coated tubes*. Trans. Am. Soc. Artif. Intern. Organs, 1982. **28**: p. 444-50.

35. Hirsh, J., *Oral Anticoagulant Drugs.* The New England Journal of Medicine, 1991. **324**(26): p. 1865-75.

36. Hirsh, J., J.E. Dalen, V. Fuster, L.B. Harker, C. Patrono and G. Roth, *Aspirin and other platelet-active drugs: the relationship among dose, effectiveness, and side effects*. Chest, 1995. **108**(4): p. 247S-57S.

37. Solen, K.A., S. Sukavaneshvar, Y. Zheng, B. Hanrahan, M.W. Hall, P. Goodman, B. Goodman and S.F. Mohammad, *A Light-Scattering Instrument to Detect Thromboemboli in Blood*. J. Biomedical Optics, 2003. **8**: p. 70-79.

38. Slack, S.M. and V.T. Turitto, *Flow chambers and their standardization for use in studies of thrombosis. On Behalf of the Subcommittee on Rheology of the Scientific and Standardization Committee of the ISTH.* Thromb Haemost, 1994. **72**(5): p. 777-81.

39. Bird, R.B, W.E. Stewart, and E. N. Lightfoot. *Transport Phenomena,* 2nd Edition. New York. John Wiley & Sons, Inc., 2002. p. 136-137.

40. Incropera, F.P., and D.P. De Witt, *Fundamentals of Heat and Mass Transfer,* 3rd Edition. 1990, John Wiley & Sons: New York. p. 491-495.

41. Hellums, J.D., *1993 Whitaker Lecture: Biorheology in Thrombosis Research.* Annals of Biomedical Engineering, 1994. **22**(5): p. 445-455.

42. Deykin, D., *Thrombogenesis*. The New England Journal of Medicine, 1967. **276**(11): p. 622-628.

43. Goodman, P., *The development of a comprehensive hemodynamic model of device-induced thromboembolism.* Ph.D. Dissertation, Brigham Young University, August 2003. p. 75

44. Andersen, B., *Multi-processor computation of thrombus growth and embolization in a model of blood-biomaterial interaction based on fluid dynamics.* M.S. Thesis, Brigham Young University, August 2012.

APPENDIX A – AN EXAMPLE OF IMAGE J BOUNDARY DATA OUTPUT

X_raw	Y_raw	Y_zeroed	Y_adjusted	X (mm)	Y (mm)
1.000	120.447	4.388	7.638	0.001	0.010
2.000	123.624	7.565	13.167	0.003	0.017
3.000	125.129	9.071	15.788	0.004	0.020
4.000	126.471	10.412	18.123	0.005	0.023
5.000	127.894	11.835	20.601	0.006	0.026
6.000	129.365	13.306	23.160	0.008	0.029
7.000	131.341	15.282	26.601	0.009	0.034
8.000	133.259	17.200	29.939	0.010	0.038
9.000	135.047	18.988	33.051	0.011	0.042
10.000	136.471	20.412	35.529	0.013	0.045
11.000	137.741	21.682	37.741	0.014	0.048
12.000	139.247	23.188	40.362	0.015	0.051
13.000	140.353	24.294	42.287	0.017	0.054
14.000	141.741	25.682	44.703	0.018	0.057
15.000	142.635	26.576	46.259	0.019	0.059
16.000	143.812	27.753	48.307	0.020	0.061
17.000	144.976	28.918	50.334	0.022	0.064
18.000	145.906	29.847	51.952	0.023	0.066
19.000	147.012	30.953	53.877	0.024	0.068
20.000	147.988	31.929	55.577	0.025	0.071
21.000	148.576	32.518	56.601	0.027	0.072
22.000	149.329	33.271	57.911	0.028	0.074
23.000	150.000	33.941	59.079	0.029	0.075
24.000	150.776	34.718	60.430	0.031	0.077
25.000	151.694	35.635	62.027	0.032	0.079
26.000	152.318	36.259	63.113	0.033	0.080
27.000	153.082	37.024	64.444	0.034	0.082
28.000	153.659	37.600	65.447	0.036	0.083
29.000	154.612	38.553	67.106	0.037	0.085
30.000	155.388	39.329	68.457	0.038	0.087
31.000	156.153	40.094	69.788	0.039	0.089
32.000	156.553	40.494	70.485	0.041	0.090
33.000	157.047	40.988	71.345	0.042	0.091

Y MIN:	116.059
Y_ZEROED MAX:	48.259
HEIGHT:	84.000
PIXELS (pixels/mm):	786.670
RATIO:	1.741

34.000	157.624	41.565	72.348	0.043	0.092
35.000	158.341	42.282	73.597	0.044	0.094
36.000	158.965	42.906	74.683	0.046	0.095
37.000	159.753	43.694	76.055	0.047	0.097
38.000	160.082	44.024	76.628	0.048	0.097
39.000	160.106	44.047	76.669	0.050	0.097
40.000	160.518	44.459	77.386	0.051	0.098
41.000	160.965	44.906	78.164	0.052	0.099
42.000	161.153	45.094	78.491	0.053	0.100
43.000	161.247	45.188	78.655	0.055	0.100
44.000	161.565	45.506	79.208	0.056	0.101
45.000	161.941	45.882	79.863	0.057	0.102
46.000	162.282	46.224	80.457	0.058	0.102
47.000	162.494	46.435	80.826	0.060	0.103
48.000	162.518	46.459	80.867	0.061	0.103
49.000	162.918	46.859	81.563	0.062	0.104
50.000	163.271	47.212	82.177	0.064	0.104
51.000	163.012	46.953	81.727	0.065	0.104
52.000	163.176	47.118	82.014	0.066	0.104
53.000	163.424	47.365	82.444	0.067	0.105
54.000	163.729	47.671	82.976	0.069	0.105
55.000	163.929	47.871	83.324	0.070	0.106
56.000	164.059	48.000	83.549	0.071	0.106
57.000	164.165	48.106	83.734	0.072	0.106
58.000	164.259	48.200	83.898	0.074	0.107
59.000	164.318	48.259	84.000	0.075	0.107
60.000	164.259	48.200	83.898	0.076	0.107
61.000	164.141	48.082	83.693	0.078	0.106
62.000	164.106	48.047	83.631	0.079	0.106
63.000	163.847	47.788	83.181	0.080	0.106
64.000	163.929	47.871	83.324	0.081	0.106
65.000	163.882	47.824	83.242	0.083	0.106
66.000	163.518	47.459	82.608	0.084	0.105
67.000	163.294	47.235	82.218	0.085	0.105
68.000	162.953	46.894	81.625	0.086	0.104
69.000	162.506	46.447	80.846	0.088	0.103
70.000	162.247	46.188	80.396	0.089	0.102
71.000	161.824	45.765	79.659	0.090	0.101
72.000	161.376	45.318	78.881	0.092	0.100
73.000	160.729	44.671	77.754	0.093	0.099
74.000	160.118	44.059	76.689	0.094	0.097

75.000	159.529	43.471	75.666	0.095	0.096
76.000	158.694	42.635	74.212	0.097	0.094
77.000	157.529	41.471	72.184	0.098	0.092
78.000	156.435	40.376	70.280	0.099	0.089
79.000	155.565	39.506	68.765	0.100	0.087
80.000	153.988	37.929	66.020	0.102	0.084
81.000	152.847	36.788	64.034	0.103	0.081
82.000	151.965	35.906	62.498	0.104	0.079
83.000	150.953	34.894	60.737	0.106	0.077
84.000	150.012	33.953	59.099	0.107	0.075
85.000	149.765	33.706	58.669	0.108	0.075
86.000	149.059	33.000	57.440	0.109	0.073
87.000	148.118	32.059	55.802	0.111	0.071
88.000	147.341	31.282	54.451	0.112	0.069
89.000	146.682	30.624	53.304	0.113	0.068
90.000	146.165	30.106	52.403	0.114	0.067
91.000	145.576	29.518	51.379	0.116	0.065
92.000	144.906	28.847	50.212	0.117	0.064
93.000	144.012	27.953	48.655	0.118	0.062
94.000	142.988	26.929	46.874	0.119	0.060
95.000	142.141	26.082	45.399	0.121	0.058
96.000	141.635	25.576	44.519	0.122	0.057
97.000	140.824	24.765	43.106	0.123	0.055
98.000	139.812	23.753	41.345	0.125	0.053
99.000	139.071	23.012	40.055	0.126	0.051
100.000	138.118	22.059	38.396	0.127	0.049
101.000	137.706	21.647	37.679	0.128	0.048
102.000	137.000	20.941	36.451	0.130	0.046
103.000	136.306	20.247	35.242	0.131	0.045
104.000	135.365	19.306	33.604	0.132	0.043
105.000	134.718	18.659	32.478	0.133	0.041
106.000	134.118	18.059	31.433	0.135	0.040
107.000	133.435	17.376	30.246	0.136	0.038
108.000	132.824	16.765	29.181	0.137	0.037
109.000	131.588	15.529	27.031	0.139	0.034
110.000	131.153	15.094	26.273	0.140	0.033
111.000	129.953	13.894	24.184	0.141	0.031
112.000	129.212	13.153	22.894	0.142	0.029
113.000	128.165	12.106	21.072	0.144	0.027
114.000	127.412	11.353	19.761	0.145	0.025
115.000	126.776	10.718	18.655	0.146	0.024

116.000	126.071	10.012	17.427	0.147	0.022
117.000	125.471	9.412	16.382	0.149	0.021
118.000	124.729	8.671	15.092	0.150	0.019
119.000	123.753	7.694	13.393	0.151	0.017
120.000	122.824	6.765	11.775	0.153	0.015
121.000	122.024	5.965	10.382	0.154	0.013
122.000	121.541	5.482	9.543	0.155	0.012
123.000	120.918	4.859	8.457	0.156	0.011
124.000	120.259	4.200	7.311	0.158	0.009
125.000	119.659	3.600	6.266	0.159	0.008
126.000	118.894	2.835	4.935	0.160	0.006
127.000	118.388	2.329	4.055	0.161	0.005
128.000	118.071	2.012	3.502	0.163	0.004
129.000	117.529	1.471	2.560	0.164	0.003
130.000	117.200	1.141	1.986	0.165	0.003
131.000	117.035	0.976	1.700	0.167	0.002
132.000	116.612	0.553	0.962	0.168	0.001
133.000	116.741	0.682	1.188	0.169	0.002
134.000	116.059	0.000	0.000	0.170	0.000

APPENDIX B – AN EXAMPLE OF THROMBUS VOLUME CALCULATION

Radius of the small tube:

$$R_{cath} := \frac{0.3mm}{2}$$

Defining the unit microliter:

$$\mu L := 10^{-6} L$$

Length of thrombus at t = 240 seconds:

$$L_{240} := 0.1656mm$$

Thrombus height boundary equation:

$$H_{240}(x) := mm \left[-200225.2 \left(\frac{x}{mm} \right)^6 + 105689.77 \left(\frac{x}{mm} \right)^5 - 20688.97 \left(\frac{x}{mm} \right)^4 + 1912.27 \left(\frac{x}{mm} \right)^3 - 104.97 \left(\frac{x}{mm} \right)^2 + 4.35 \frac{x}{mm} \right]$$

Cross-sectional area of thrombus at x:

$$A_{csthrom240}(x) := 2 \cdot \left[\left[R_{cath}^{\ 2} \cdot \operatorname{acos}\left(\frac{R_{cath} - 0.5 \cdot H_{240}(x)}{R_{cath}} \right) - \left(R_{cath} - 0.5 \cdot H_{240}(x) \right) \cdot \left(\sqrt{R_{cath} \cdot H_{240}(x) - 0.25 \cdot H_{240}(x)^2} \right) \right] \right]$$

Volume of Thrombus at t = 240 seconds

$$V_{throm240}(l) := \int_0^l A_{csthrom240}(x)\, dx$$

$$V_{throm240}(L_{240}) = 1.457 \times 10^{-3} \cdot \mu L$$

APPENDIX C – AN EXAMPLE OF SHEAR STRESS AND EXPOSURE TIME FOR HELLUMS'S CURVE TEST

Early stages of thrombus growth

$\tau_0 := 18.563Pa$ Shear Stress at the highest point of thrombus height.
This is part of shear force calculation - See Appendix D

$\tau_0 = 185.63 \cdot \frac{dyne}{cm^2}$

$ExposureTime = \frac{L}{V_{avg}}$ L is the length of thrombus

Average Velocity = Volumetric Flow Rate / Cross Section Area of Blood Flow

$L_0 := 0.04mm$ Length of Throms at t = 0.

$A_{bloodflow0} := 6.99 \cdot 10^{-8} m^2$ From Shear Force Calculation - See Appendix D

$Vol := 1 \frac{mL}{min}$

$ExposureTime_0 := \frac{L_0}{\frac{Vol}{A_{bloodflow0}}}$ $ExposureTime_0 = 1.678 \times 10^{-4} s$

Late stages of thrombus growth

$\tau_{210} := 41.014Pa$ $\tau_{210} = 410.14 \cdot \frac{dyne}{cm^2}$ $L_{210} := 0.31mm$

$A_{bloodflow210} := 1.702 \cdot 10^{-8} m^2$

$ExposureTime_{210} := \frac{L_{210}}{\frac{Vol}{A_{bloodflow210}}}$ $ExposureTime_{210} = 3.166 \times 10^{-4} s$

APPENDIX D – AN EXAMPLE OF SHEAR FORCE ACTING ON A THROMBUS

Radius of the small tube:

$$R_{cath} := \frac{0.3\,mm}{2}$$

Defining the unit microliter:

$$\mu L := 10^{-6} L$$

Length of thrombus at t = 240 seconds:

$$L_{240} := 0.1656\,mm$$

Thrombus height boundary equation:

$$H_{240}(x) := mm\left[-200225.2\cdot\left(\frac{x}{mm}\right)^6 + 105689.77\cdot\left(\frac{x}{mm}\right)^5 - 20688.97\cdot\left(\frac{x}{mm}\right)^4 + 1912.27\cdot\left(\frac{x}{mm}\right)^3 - 104.97\left(\frac{x}{mm}\right)^2 + 4.35\,\frac{x}{mm}\right]$$

Cross-sectional area of thrombus at x:

$$A_{csthrom240}(x) := 2\cdot\left[\left[R_{cath}^{\,2}\cdot\operatorname{acos}\left(\frac{R_{cath} - 0.5\cdot H_{240}(x)}{R_{cath}}\right) - \left(R_{cath} - 0.5\cdot H_{240}(x)\right)\cdot\left(\sqrt{R_{cath}\cdot H_{240}(x) - 0.25\cdot H_{240}(x)^2}\right)\right]\right]$$

Cross-sectional area of blood flow at x:

$$A_{bloodflow240}(x) := \pi\cdot R_{cath}^{\,2} - A_{csthrom240}(x) \qquad A_{bloodflow240}(L_{240}) = 0.071\cdot mm^2$$

Volumetric Flow Rate:

$$V_{bloodflow} := 1\,\frac{mL}{min}$$

Viscosity of Blood:

$$\mu := .0032\,Pa\cdot s$$

Density of Blood:

$$\rho_{blood} := 1060\,\frac{kg}{m^3}$$

Kinematic Viscosity of Blood:

$$\nu := \frac{\mu}{\rho_{blood}}$$

Boundary-layer Thickness of Blood Flow through a Passage Partially Obstructed by the Thrombus:

$$\delta_{240}(x) := 4.64\cdot\sqrt{\frac{\nu\cdot x}{\frac{V_{bloodflow}}{A_{bloodflow240}(x)}}}$$

Perimeter of the Thrombus Cross-Section:

$$P_{240}(x) := 2 \cdot R_{cath} \cdot \operatorname{acos}\left(1 - \frac{H_{240}(x)}{2R_{cath}}\right)$$

Shear Stress Across the Surface of the Thrombus:

$$\tau_{240f}(x) := \frac{R_{cath} - H_{240}(x)}{R_{cath}}\left[\mu \cdot \frac{4 \cdot \left(R_{cath} - H_{240}(x)\right) \cdot \frac{V_{bloodflow}}{A_{bloodflow240}(x)}}{R_{cath}^{\,2}}\right] + \frac{H_{240}(x)}{R_{cath}}\left(\mu \cdot \frac{3 \cdot \frac{V_{bloodflow}}{A_{bloodflow240}(x)}}{2 \cdot \delta_{240}(x)}\right)$$

Shear Force on the Surface of the Thrombus:

$$F_{shear240}(l) := \int_{0.00001mm}^{l} \tau_{240f}(x) \cdot P_{240}(x)\, dx$$

$$F_{shear240}(L_{240}) = 3.898 \times 10^{-7} N$$

APPENDIX E – AN EXAMPLE OF THROMBUS ADHESION STRENGTH CALCULATION

According to High-Definition Video, the Thrombus Embolizes at t = 393 seconds.

The Shear Force at Embolization, t = 393 seconds is:

$$F_{shear393} := 6.154 \times 10^{-7} N$$

Surface Area of Thrombus-Biomateria:

$$A_{surface393}(L_{393}) = \int_{0.00001\,mm}^{l} P_{393}(x)\,dx$$

$$A_{surface393} := 4.73 \times 10^{-8}\ m^2$$

Adhesion Strength of Thrombus:

$$AdhesionStrength := \frac{F_{shear393}}{A_{surface393}}$$

$$AdhesionStrength = 13.011 \cdot \frac{N}{m^2}$$